A TOPOLOGICAL PERSPECTIVE ON DEMYSTIFYING GNN-BASED LINK PREDICTION PERFORMANCE

Yu Wang[1], **Tong Zhao**[2], **Yuying Zhao**[1], **Yunchao Liu**[1], **Xueqi Cheng**[1], **Neil Shah**[2], **Tyler Derr**[1]
[1]Vanderbilt University [2]Snap Inc.
`{yu.wang.1,yuying.zhao,yunchao.liu,xueqi.cheng,tyler.derr}@vanderbilt.edu`
`{tzhao,nshah}@snap.com`

ABSTRACT

Graph Neural Networks (GNNs) have shown great promise in learning node embeddings for link prediction (LP). While numerous studies improve the overall GNNs' LP performance, none have explored their varying performance across different nodes and the underlying reasons. To this end, we demystify which nodes perform better from the perspective of their local topology. Despite the widespread belief that low-degree nodes exhibit worse LP performance, we surprisingly observe an inconsistent performance trend. This prompts us to propose a node-level metric, Topological Concentration (TC), based on the intersection of the local subgraph of each node with the ones of its neighbors. We empirically demonstrate that TC correlates with LP performance more than other node-level topological metrics, better identifying low-performing nodes than using degree. With TC, we discover a novel topological distribution shift issue in which nodes' newly joined neighbors tend to become less interactive with their existing neighbors, compromising the generalizability of node embeddings for LP at testing time. To make the computation of TC scalable, We further propose Approximated Topological Concentration (ATC) and justify its efficacy in approximating TC with reduced computation complexity. Given the positive correlation between node TC and its LP performance, we explore the potential of boosting LP performance via enhancing TC by re-weighting edges in the message-passing and discuss its effectiveness with limitations. Our code is publicly available at https://github.com/YuWVandy/Topo_LP_GNN.

1 INTRODUCTION

Recent years have witnessed unprecedented success in applying link prediction (LP) in real-world applications (Ying et al., 2018; Rozemberczki et al., 2022). Compared with heuristic-based (Brin & Page, 1998; Liben-Nowell & Kleinberg, 2003) and shallow embedding-based LP approaches (Perozzi et al., 2014; Grover & Leskovec, 2016), GNN-based ones (Zhang & Chen, 2018; Chamberlain et al., 2022) have achieved state-of-the-art (SOTA) performance; these methods first learn node/subgraph embeddings by applying linear transformations with message-passing and a decoder/pooling layer to predict link scores/subgraph class. While existing works are dedicated to boosting overall LP performance (Zhao et al., 2022; Chen et al., 2021b) by more expressive message-passing or data augmentation, it is heavily under-explored whether different nodes within a graph would obtain embeddings of different quality and have varying LP performance.

Previous works have explored GNNs' varying performance on nodes within a graph, considering factors like local topology (e.g., degree and homophily/heterophily) (Tang et al., 2020; Mao et al., 2023), feature quality (Taguchi et al., 2021), and class quantity (Zhao et al., 2021a). While these studies have provided significant insights, their focus has primarily remained on node/graph-level tasks, leaving the realm of LP unexplored. A more profound examination of the node-varying LP performance can enhance our comprehension of network dynamics (Liben-Nowell & Kleinberg, 2003), facilitate timely detection of nodes with ill-topology (Lika et al., 2014), and inspire customized data augmentation for different nodes (Zhao et al., 2021b). Recognizing the criticality of studying the node-varying LP performance and the apparent gap in the existing literature, we ask:

Can we propose a metric that measures GNNs' varying LP performance across different nodes?

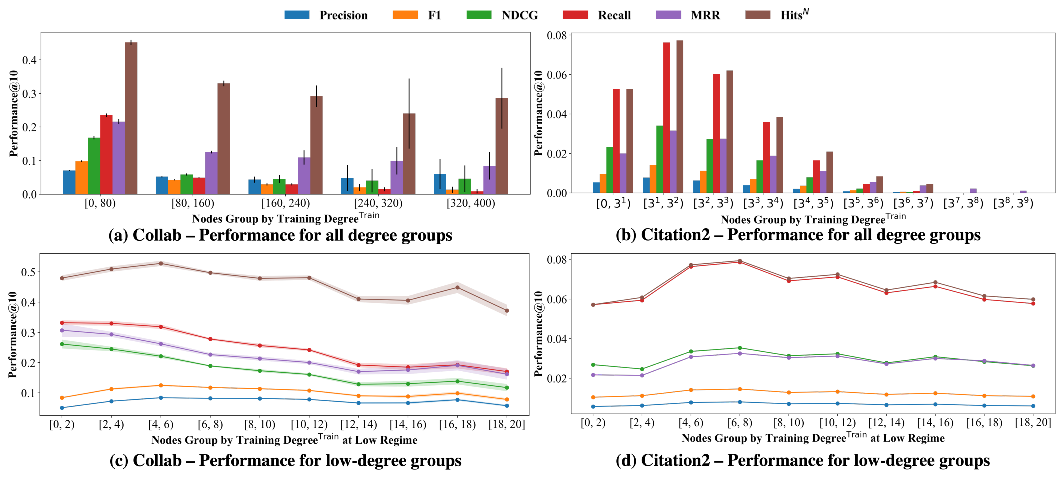

Figure 1: Average LP performance of nodes across different degree groups based on Degree$^{\text{Train}}$(i.e., node degree by training edges) on Collab/Citation2. In **(a)-(b)**, Performance@10 does not increase as the node degree increases. In **(c)-(d)**, few/lower-degree nodes do not perform worse than their higher-degree counterparts. Detailed experimental setting is included in Appendix F

To answer an analogous question in node classification, prior works observed that GNNs perform better on high-degree nodes than low-degree nodes (Tang et al., 2020; Liu et al., 2021). Similarly, the persistent sparse topology issue in the general LP domain and recommender systems (Hao et al., 2021; Li et al., 2021) indicates that nodes with zero-to-low degrees lag behind their high-degree counterparts. However, as surprisingly shown in Figure 1(a)-(b), GNN-based LP on these two large-scale social networks does not exhibit a consistent performance trend as the node degree increases. For example, the performance@10 on Collab under all evaluation metrics decreases as the node degree increases, while on Citation2, performance@10 first increases and then decreases. This counter-intuitive observation indicates the weak correlation between the node degree and LP performance, which motivates us to design a more correlated metric to answer the above question.

Following (Zhang & Chen, 2018) that the link formation between each pair of nodes depends on the interaction between their local subgraphs, we probe the relation between the local subgraphs around each node and its GNN-based LP performance. Specifically, we propose Topological Concentration (TC) and its scalable version, Approximated Topological Concentration (ATC), to measure the topological interaction between the local subgraph of each node and the local subgraphs of the neighbors of that node. Our empirical observations show that TC offers a superior characterization of node LP performance in GNNs, leading to 82.10% more correlation with LP performance and roughly 200% increase in the performance gap between the identified under-performed nodes and their counterparts than degree. Moreover, with TC, we discover a novel topological distribution shift (TDS) in which newly joined neighbors of a node tend to become less interactive with that node's existing neighbors. This TDS would compromise the generalizability of the learned node embeddings in LP at the testing time. Given the closer correlation between TC and LP performance, we reweigh the edges in message-passing to enhance TC and discuss its efficacy/limitations in boosting LP performance. Our contributions are summarized as follows:

- We propose Topological Concentration (TC) and demonstrate it leads to 82.10% more correlation with LP performance and roughly 200% increase in the performance gap between the identified under-performed nodes and their counterparts than node degree, shedding new insights on degree-related issues in LP. We further propose Approximated Topological Concentration (ATC) and demonstrate it maintains high correlations to the LP performance similar to TC while significantly reducing the computation complexity.
- We uncover a novel Topological Distribution Shift (TDS) issue according to TC and demonstrate its negative impact at the node/graph level for link prediction at the testing time. Moreover, we discover that different nodes within the same graph can have varying amounts of TDS.
- We design a TC-inspired message-passing where a node aggregates more from neighbors that have more connections to the local subgraph of that node, which can enhance the node's weighted TC. We observe this empirically boosts LP performance and lastly discuss its noncausal limitations.

2 Related work

Varying Performance of GNNs on Node/Graph Classification. GNNs' efficacy in classification differs across nodes/graphs with varying label quantity (e.g., imbalanced node/graph classification (Zhao et al., 2021a; Wang et al., 2022b)) and varying topology quality (e.g., long-tailed (Tang et al., 2020; Liu et al., 2021)/heterophily node classification (Zhu et al., 2020; Mao et al., 2023)). To enhance GNNs' performance for the disadvantaged nodes/graphs in these two varying conditions, previous works either apply data augmentations to derive additional supervision (Wang et al., 2021; Park et al., 2021) or design expressive graph convolutions to mitigate structural bias (Zhu et al., 2021; Han et al., 2023). However, none of them tackle the varying performance of nodes in LP. We fill this gap by studying the relationship between node LP performance and its local topology.

GNN-based LP and Node-Centric Evaluation. GNN-based LP works by first learning node embeddings/subgraph embeddings through linear transformation and message-passing, and then applying the scoring function to predict link probability/subgraph class (Zhang & Chen, 2018; Yin et al., 2022; Wang et al., 2022c; Tan et al., 2023). It has achieved new SOTA performance owing to using the neural network to extract task-related information and the message-passing to encode the topological properties (e.g., common neighbors) (Yun et al., 2021; Chamberlain et al., 2022). Existing GNN-based LP baselines evaluate performance by computing the average rank of each link against the randomly sampled negative links (Hu et al., 2020). However, because these sampled negative links only count a tiny portion of the quadratic node pairs, this evaluation contains positional bias (Li et al., 2023). In view of this issue, we leverage the node-centric evaluation metrics (Precision/F1/NDCG/Recall/Hits^N@K) that are frequently used in recommender systems (Gori et al., 2007; He et al., 2020) and rank each node against all other nodes in predicting the incoming neighbors. Detailed definitions of these evaluation metrics are provided in Appendix C.

Varying Performance of GNNs on LP. As LP nowadays has been heavily used to enhance user experience in social/e-commerce recommendations (Fan et al., 2019; Zhao et al., 2023), studying its varying performance across different users has real-world applications Zhao et al. (2024) such as identifying users with ill-topology. Although no efforts have been investigated into the node-varying performance in GNN-based LP, prior work (Li et al., 2021; Rahmani et al., 2022; Guo et al., 2024) have investigated the relation of node-varying LP performance with its degree, and both claimed that users/nodes with higher activity levels/degrees tend to possess better recommendation performance than their less active counterparts, which also aligns with observations in GNN-based node classification (Tang et al., 2020; Liu et al., 2021). However, Figure 1(c)-(d) has already raised concern over the validity of this claim in LP. We follow (Wang & Derr, 2022) and theoretically discover that some node-centric evaluation metrics have degree-related bias in Appendix D.2, implying that the GNNs' varying LP performance could be partially attributed to the choice of evaluation metrics. To mitigate this bias, we employ a full spectrum of evaluation metrics and find that degree is not so correlated with the node LP performance. This motivates us to devise a better topological metric than the degree. Note that although some prior works also define cold-start nodes to be the ones with few degrees, we systematically review their connections and differences in Appendix B.

3 Topological Concentration

3.1 Notations

Let $G = (\mathcal{V}, \mathcal{E}, \mathbf{X})$ be an attributed graph, where $\mathcal{V} = \{v_i\}_{i=1}^n$ is the set of n nodes (i.e., $n = |\mathcal{V}|$) and $\mathcal{E} \subseteq \mathcal{V} \times \mathcal{V}$ is the set of m observed training edges (i.e., $m = |\mathcal{E}|$) with e_{ij} denoting the edge between the node v_i and v_j, and $\mathbf{X} \in \mathbb{R}^{n\times d}$ represents the node feature matrix. The observed adjacency matrix of the graph is denoted as $\mathbf{A} \in \{0, 1\}^{n\times n}$ with $\mathbf{A}_{ij} = 1$ if an observed edge exists between node v_i and v_j and $\mathbf{A}_{ij} = 0$ otherwise. The diagonal matrix of node degree is notated as $\mathbf{D} \in \mathbb{Z}^{n\times n}$ with the degree of node v_i being $d_i = \mathbf{D}_{ii} = \sum_{j=1}^n \mathbf{A}_{ij}$. For the LP task, edges are usually divided into three groups notated as $\mathcal{T} = \{\text{Train}, \text{Val}, \text{Test}\}$, i.e., training, validation, and testing sets, respectively. We denote $\mathcal{N}_i^t, t \in \mathcal{T}$ as node v_i's 1-hop neighbors according to edge group t. Furthermore, we denote the set of nodes that have at least one path of length k to node i based on observed training edges as $\mathcal{H}_i^k$ and naturally $\mathcal{H}_i^1 = \mathcal{N}_i^{\text{Train}}$. Note that $\mathcal{H}_i^{k_1} \cap \mathcal{H}_i^{k_2}$ is not necessarily empty since neighbors that are k_1-hops away from v_i could also have paths of length k_2 reaching v_i. We collect v_i's neighbors at all different hops until K to form the K-hop computation tree centered on v_i as $\mathcal{S}_i^K = \{\mathcal{H}_i^k\}_{k=1}^K$. We summarize all notations in Table 2 in Appendix A.

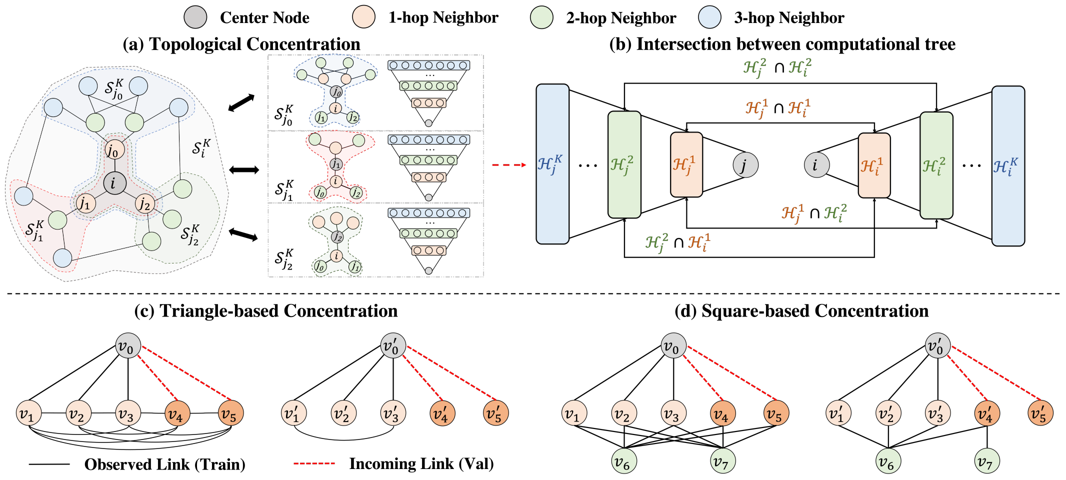
Center Node
1-hop Neighbor
2-hop Neighbor
3-hop Neighbor
(a) Topological Concentration
(b) Intersection between computational tree
(c) Triangle-based Concentration
(d) Square-based Concentration
Observed Link (Train)
Incoming Link (Val)

Figure 2: **(a)-(b)**: v_i's Topological Concentration: we calculate the average intersection between v_i's computation tree and each of v_i's neighbor's computation tree. The intersection between two computation trees is the ratio of the observed intersections to all possible intersections. **(c)-(d)**: two specifications of TC, corresponding to social and e-commerce networks. A higher triangle/square-based concentration indicates more triangles/squares are formed among v_0's local subgraph.

3.2 Topological Concentration: Intuition and Formalization

As the link formation between a node pair heavily depends on the intersection between their local subgraphs (Zhang & Chen, 2018; Chamberlain et al., 2022), we similarly hypothesize that the predictability of a node's neighbors relates to the intersection between this node's subgraph and the subgraphs of that node's neighbors, e.g., the prediction of the links $\{(i, j_k)\}_{k=0}^2$ in Figure 2(a) depends on the intersection between $\mathcal{S}_i^K$ and $\{\mathcal{S}_{j_k}^K\}_{k=0}^2$. A higher intersection leads to higher LP performance. For example, in Figure 2(c)-(d), v_0 neighbors closely interact with themselves while v_0' neighbors do not, posing different topological conditions for the LP on v_0 and v_0'. From graph heuristics perspective, v_0 shares common neighbors v_1, v_2, v_3 with its incoming validation neighbors v_4, v_5 while v_0' shares no neighbors with v_4', v_5'. From the message-passing perspective, the propagated embeddings of v_0 and v_4, v_5 share common components since they all aggregate $\{v_k\}_{k=1}^3$ embeddings while v_0' and v_4', v_5' do not share any common embeddings among $\{v_k'\}_{k=1}^3$. When the subgraph (i.e., computation tree) surrounding a node increasingly overlaps with the subgraphs of its neighbors, more paths originating from that node are likely to loop nearby and eventually return to it, resulting in a more dense/concentrated local topology for that node. Inspired by this observation, we introduce *Topological Concentration* to measure the average level of intersection among these local subgraphs as follows:

Definition 1. ***Topological Concentration (TC):*** *The Topological Concentration $C_i^{K,t}$ for node $v_i \in \mathcal{V}$ is defined as the average intersection between v_i's K-hop computation tree ($\mathcal{S}_i^K$) and the computation trees of each of v_i's type t neighbors:*

$$C_i^{K,t} = \mathbb{E}_{v_j \sim \mathcal{N}_i^t} I(\mathcal{S}_i^K, \mathcal{S}_j^K) = \mathbb{E}_{v_j \sim \mathcal{N}_i^t} \frac{\sum_{k_1=1}^K \sum_{k_2=1}^K \beta^{k_1+k_2-2} |\mathcal{H}_i^{k_1} \cap \mathcal{H}_j^{k_2}|}{\sum_{k_1=1}^K \sum_{k_2=1}^K \beta^{k_1+k_2-2} g(|\mathcal{H}_i^{k_1}|, |\mathcal{H}_j^{k_2}|)} \quad (1)$$

$\forall v_i \in \mathcal{V}, \forall t \in \mathcal{T}$, where $I(\mathcal{S}_i^K, \mathcal{S}_j^K)$ quantifies the intersection between the K-hop computation trees around v_i and v_j, and is decomposed into the ratio of the observed intersections $|\mathcal{H}_i^{k_1} \cap \mathcal{H}_j^{k_2}|$ to the total possible intersections $g(\mathcal{H}_i^{k_1}, \mathcal{H}_j^{k_2})$ between neighbors that are k_1 and k_2 hops away as shown in Figure 2(b). $\beta^{k_1+k_2-2}$ accounts for the exponential discounting effect as the hop increases. The normalization term g is a function of the size of the computation trees of node v_i, v_j (Fu et al., 2022). Although computation trees only consist of edges from the training set, v_i's neighbors $\mathcal{N}_i^t$ in Eq. (1) could come from training/validation/testing sets, and we term the corresponding TC as TC$^{\text{Train}}$, TC$^{\text{Val}}$, TC$^{\text{Test}}$ and their values as $C_i^{K,\text{Train}}$, $C_i^{K,\text{Val}}$, $C_i^{K,\text{Test}}$. We verify the correlation between TC and the node LP performance in Section 3.3.

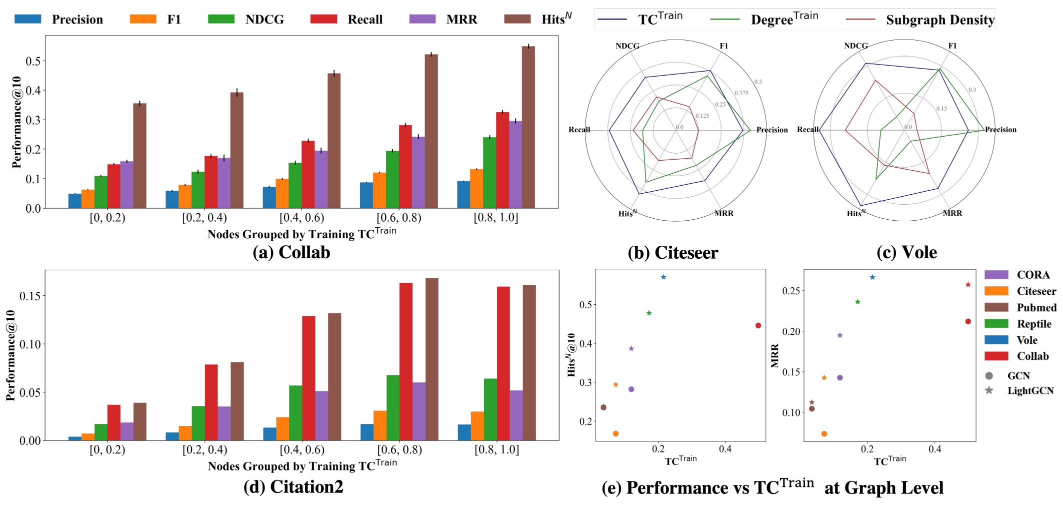

Figure 3: **(a)/(d)**: The average LP Performance of nodes on Collab/Citation2 monotonically increases as the TC^{Train} increases. **(b)/(c)**: TC^{Train} mostly achieves the highest Pearson Correlation with LP performance on Citeseer/Vole than $\text{Degree}^{\text{Train}}$ and Subgraph Density metrics. **(e)**: LP performance is positively correlated to TC^{Train} across different network datasets. The deviation of Collab under both GCN and LightGCN baselines from the primary linear trend might be attributed to the duplicated edges in the network that create the illusion of a higher TC^{Train}.

3.3 Topological Concentration: Observation and Analysis

In this section, we draw three empirical observations to delve into the role of TC in GNN-based LP. For all experiments, we evaluate datasets with only the topology information using LightGCN and those also with node features using GCN/SAGE (Kipf & Welling, 2016; Hamilton et al., 2017; He et al., 2020)[1]. Detailed experimental settings are described in Appendix F. Please note that while the findings illustrated in this section are limited to the presented datasets due to page limitation, more comprehensive results are included in Appendix G.

Obs. 1. TC correlates to LP performance more than other node topological properties. In Figure 3 (a)/(d), we group nodes in Collab/Citation2 based on their TC^{Train} and visualize the average performance of each group. Unlike Figure 1(a)/(b), where there is no apparent relationship between the performance and the node degree, the performance almost monotonically increases as the node TC^{Train} increases regardless of the evaluation metrics. This demonstrates the capability of TC^{Train} in characterizing the quality of nodes' local topology for their LP performance. Moreover, we quantitatively compare the Pearson Correlation of the node LP performance with TC^{Train} and other commonly used node local topological properties, $\text{Degree}^{\text{Train}}$ (i.e., the number of training edges incident to a node) and SubGraph Density (i.e., the density of the 1-hop training subgraph centering around a node). As shown in Figure 3(b)/(c), TC^{Train} almost achieves the highest Pearson Correlation with the node LP performance across every evaluation metric than the other two topological properties except for the precision metric. This is due to the degree-related evaluation bias implicitly encoded in the precision metric, i.e., even for the untrained link predictor, the precision of a node still increases linearly as its degree increases, as proved in Theorem 3. Note that the node's 1-hop Subgraph Density equals its local clustering coefficient (LCC), and one previous work (Pan et al., 2022) has observed its correlation with node LP performance. To justify the advantages of TC^{Train} over LCC, we provide a concrete example in Appendix E. Additionally, Figure 3(e) shows that TC^{Train} also positively correlated with LP performance across various networks, depicting a preliminary benchmark for GNNs' LP performance at the graph level (Palowitch et al., 2022). The LightGCN architecture exhibits a steeper slope than GCN, as it relies exclusively on network topology without leveraging node features and thus is more sensitive to changes in the purely topological metric, TC. The deviation of Collab under both GCN and LightGCN baselines from the primary linear trend might be attributed to the duplicated edges in the network that create the illusion of a higher TC^{Train} (Hu et al., 2020).

[1]Due to GPU memory limitation, we choose SAGE for Citation2.

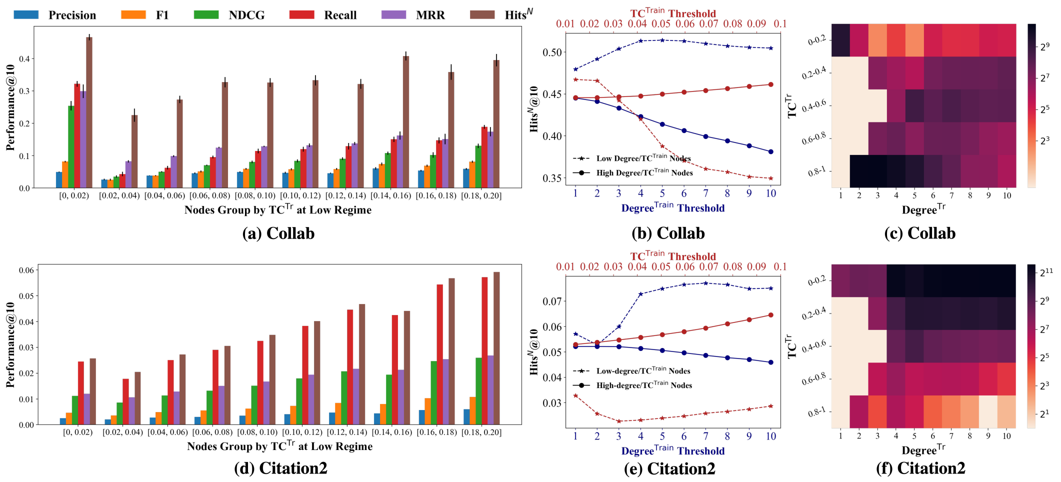

(a) Collab (b) Collab (c) Collab

(d) Citation2 (e) Citation2 (f) Citation2

Figure 4: **(a)/(d)**: The average LP performance of nodes with extremely low TC^{Train} on Collab/Citation2 almost monotonically increases as TC^{Train} increases. **(b)/(e)**: Nodes with lower $\text{Degree}^{\text{Train}}$ surprisingly perform better than their higher degree counterparts (**Blue** curves). In contrast, non-concentrated nodes identified by owning lower TC^{Train} in most cases perform worse than their concentrated counterparts (**Red** curves). **(c)/(f)**: As node $\text{Degree}^{\text{Train}}$ increases, the ratio of nodes owning higher TC^{Train} increases first and then decreases, corresponding to the observed first-increasing-and-then-decreasing performance trend in Figure 1(c)/(d).

Obs. 2. TC better identifies low-performing nodes than degree, and lower-degree nodes may not necessarily have lower LP performance.

As previously shown in Figure 1(c)/(d), when the node degree is at the very low regime, we do not observe a strict positive relationship between node $\text{Degree}^{\text{Train}}$ and its LP performance. For example, the node Recall/MRR/NDCG@10 in Collab decreases as $\text{Degree}^{\text{Train}}$ increases and Hits^{N}/F1/Precision@10 first increases and then decreases. These contradicting observations facilitate our hypothesis that the degree might not fully capture the local topology in characterizing the underperforming nodes. Conversely, in Figure 4(a)/(d) on Collab/Citation2, nodes with lower TC^{Train} almost always have worse LP performance under all evaluation metrics except when TC^{Train} is between $[0, 0.02)$. For this extreme case, we ascribe it to the distribution shift as nodes with extremely low TC^{Train} generally have a decent TC^{Test} (shown in Figure 20) and sustain a reasonable LP performance. We thoroughly investigate this distribution shift issue in **Obs. 3**. Furthermore, we select nodes with $\text{Degree}^{\text{Train}}$ from 1 to 10 and group them into 'Lower-degree/Higher-degree'. Similarly, we select nodes with TC^{Train} from 0.01 to 0.1 and group them into 'Concentrated/Non-Concentrated'. We compare their average LP performance on Collab/Citation2 in Figure 4(b)/(e). Intriguingly, Lower-degree nodes always perform better than their Higher-degree counterparts across all $\text{Degree}^{\text{Train}}$ thresholds. This brings nuances into the conventional understanding that nodes with a weaker topology (lower degree) would yield inferior performance (Li et al., 2021; Tang et al., 2020; Liu et al., 2021). In contrast, with our defined TC^{Train}, non-concentrated nodes (lower TC^{Train}) generally underperform by a noticeable margin than their concentrated counterparts (higher TC^{Train}).

We further visualize the relation between $\text{Degree}^{\text{Train}}$ and TC^{Train} in Figure 4(c)/(f). When node $\text{Degree}^{\text{Train}}$ increases from 1 to 4, the ratio of nodes owning higher TC^{Train} also increases because these newly landed nodes start forming interactions and create their initial topological context. Since we have already observed the positive correlation of TC^{Train} to nodes' LP performance previously, the LP performance under some evaluation metrics also increases as the $\text{Degree}^{\text{Train}}$ initially increases from 0 to 4 observed in Figure 1(c)/(d). When $\text{Degree}^{\text{Train}}$ increases further beyond 5, the ratio of nodes owning higher TC^{Train} gradually decreases, leading to the decreasing performance observed in the later stage of Figure 1(c)/(d). This decreasing TC^{Train} is because, for high $\text{Degree}^{\text{Train}}$ nodes, their neighbors are likely to lie in different communities and share fewer connections among themselves. For example, in social networks, high-activity users usually possess diverse relations in different online communities, and their interacted people are likely from significantly different domains and hence share less common social relations themselves Zhao et al. (2021c; 2024).

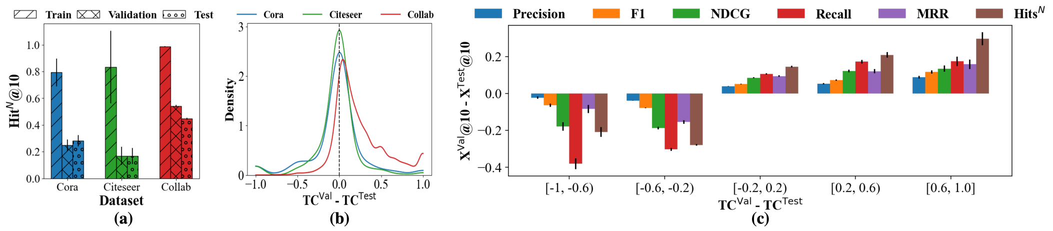

Figure 5: **(a)** Hits^N@10 of predicting training/validation/testing edges on Cora/Citeseer/Collab. The gap between validation and testing performance is much bigger on Collab than on Cora/Citeseer. **(b)** Compared with Cora/Citeseer where edges are randomly split, the distribution of the difference between TC$^{\text{Val}}$ and TC$^{\text{Test}}$ shifts slightly right on Collab where edges are split according to time, indicating the interaction between training and testing neighbors become less than the one between training and validation neighbors. **(c)** As the gap between TC$^{\text{Val}}$ and TC$^{\text{Test}}$ increases for different nodes, their corresponding performance gap also increases, demonstrating TDS varies among different nodes even within the same graph.

Obs. 3. Topological Distribution Shift compromises the LP performance at testing time, and TC can measure its negative impact at both graph and node level. In real-world LP scenarios, new nodes continuously join the network and form new links with existing nodes, making the whole network evolve dynamically (Ma et al., 2020; Rossi et al., 2020). *Here, we discover a new Topological Distribution Shift (TDS) issue, i.e., as time goes on, the newly joined neighbors of a node become less interactive with that node's old neighbors.* Since the edges serving message-passing and providing supervision only come from the training set, TDS would compromise the capability of the learned node embeddings for predicting links in the testing set. As verified in Figure 5(a), the performance gap between validation and testing sets on Collab where edges are split according to time is much more significant than the one on Cora/Citeseer where edges are split randomly. Note that the significantly higher performance on predicting training edges among all these three datasets is because they have already been used in the training phase (Wang et al., 2023), and this distribution shift is different from TDS. As TC essentially measures the interaction level among neighbors of a particular node, we further visualize the distribution of the difference between TC$^{\text{Val}}$ and TC$^{\text{Test}}$ in Figure 5(b). We observe a slight shift towards the right on Collab rather than on Cora/Citeseer, demonstrating nodes' testing neighbors become less interactive with their training neighbors than their validation neighbors. Figure 4(c) further demonstrates the influence of this shift at the node level by visualizing the relationship between TDS and the performance gap. We can see that as the strength of such shift increases (evidenced by the larger difference between TC$^{\text{Val}}$ and TC$^{\text{Test}}$), the performance gap also increases. This suggests that nodes within the same graph display varying levels of TDS. As one potential application, we can devise adaptive data valuation techniques or message-passing mechanisms to selectively use neighborhood information (i.e., emphasize less on stale edges in LP as Chamberlain et al. (2022) did). We demonstrate one use-case in Appendix K.

3.4 Topological Concentration: Computational Complexity and Optimization

Calculating TC following Eq. (1) involves counting the intersection between two neighboring sets that are different hops away from the centering nodes in two computation trees. Assuming the average degree of the network is $\widehat{d}$, the time complexity of computing $C_i^{K,t}$ for all nodes in the network is $\mathcal{O}(|\mathcal{E}|\sum_{k=1}^{K}\sum_{k=1}^{K}\min(\widehat{d}^{k_1}, \widehat{d}^{k_2})) = \mathcal{O}(K^2|\mathcal{E}||\mathcal{V}|) \approx \mathcal{O}(K^2|\mathcal{V}|^2)$ for sparse networks, which increases quadratically as the size of the network increases and is hence challenging for large-scale networks. To handle this issue, we propagate the randomly initialized Gaussian embeddings in the latent space to approximate TC in the topological space and propose *Approximated Topological Concentration* as follows:

Definition 2. ***Approximated Topological Concentration (ATC):*** *Approximated topological concentration $\widetilde{C}_i^{K,t}$ for $v_i \in \mathcal{V}$ is the average similarity between v_i and its neighbors' embeddings initialized from Gaussian Random Projection (Chen et al., 2019) followed by row-normalized graph diffusion $\widetilde{\mathbf{A}}^k$ (Gasteiger et al., 2019), with ϕ as the similarity metric function:*

$$\widetilde{C}_i^{K,t} = \mathbb{E}_{v_j \sim \mathcal{N}_i^t}\phi(\mathbf{N}_i, \mathbf{N}_j), \quad \mathbf{N} = \sum_{k=1}^{K}\alpha_k\widetilde{\mathbf{A}}^k\mathbf{R}, \quad \mathbf{R} \sim \mathcal{N}(\mathbf{0}^d, \mathbf{\Sigma}^d) \tag{2}$$

Theorem 1. *Assuming $g(|\mathcal{H}_i^{k_1}|, |\mathcal{H}_j^{k_2}|) = |\mathcal{H}_i^{k_1}||\mathcal{H}_j^{k_2}|$ in Eq. (1) and let ϕ be the dot-product based similarity metric (He et al., 2020), then node v_i's 1-layer Topological Concentration $C_i^{1,t}$ is linear correlated with the mean value of the 1-layer Approximated Topological Concentration $\mu_{\widetilde{C}_i^{K,t}}$ as:*

$$C_i^{1,t} \approx d^{-1}\mu_{\mathbb{E}_{v_j \sim \mathcal{N}_i^t}(\mathbf{E}_j^1)^\top \mathbf{E}_i^1} = d^{-1}\mu_{\widetilde{C}_i^{1,t}}, \tag{3}$$

where $\mathbf{E}^1 \in \mathbb{R}^{n \times d}$ denotes the node embeddings after 1-layer SAGE-style message-passing and d is the embedding dimension. The full proof is in Appendix D. *This theorem bridges the gap between TC defined in the topological space and ATC defined in the latent space, which theoretically justifies the effectiveness of this approximation.* Computationally, obtaining node embeddings $\mathbf{N}$ in Eq. (2) is free from optimization, and the graph diffusion can be efficiently executed via power iteration, which reduces the complexity to $\mathcal{O}(Kd(|\mathcal{E}| + |\mathcal{V}|))$. Note that although we only demonstrate the approximation power for the case of 1-layer message-passing, we empirically verify the efficacy for higher-layer message-passing in the following.

We compare TC^{Train} and $\text{ATC}^{\text{Train}}$ under various number of hops in terms of their computational time and their correlation with LP performance in Figure 6. As the number of hops increases, the running time for computing TC increases exponentially (especially for large-scale datasets like Collab, we are only affordable to compute its TC^{Train} up to 3 hops) while ATC stays roughly the same. This aligns with the quadratic/linear time complexity $\mathcal{O}(K^2|\mathcal{V}|^2)$/$\mathcal{O}(Kd(|\mathcal{E}|+|\mathcal{V}|))$ we derived earlier for TC/ATC. Moreover, ATC achieves a similar level of correlation to TC at all different hops. For both TC and ATC, their correlations to LP performance increase as the number of hops K used in Eq. (1)-Eq. (2) increases. This is because larger K enables us to capture intersections among larger subgraphs and hence accounts for more common neighbor signals (Chamberlain et al., 2022). We include comprehensive analysis including $\text{(A)TC}^{\text{Val}}$/$\text{(A)TC}^{\text{Test}}$ in Appendix J.

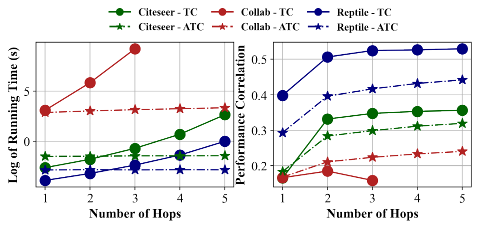

Figure 6: $\text{ATC}^{\text{Train}}$ maintains a similar level of correlation to TC^{Train} while significantly reducing the computational time.

4 Topological Concentration: Boosting GNNs' LP performance

From the aforementioned observations, TC consistently exhibits a stronger correlation with GNNs' LP performance than other commonly used node topological metrics. This insight motivates us to explore the potential of boosting GNNs' LP performance via enhancing TC^{Train}. Specifically, we propose to vary the edge weight used in message-passing by aggregating more information from neighbors that contribute more to TC^{Train}. We theoretically prove this way could enhance 1-layer TC^{Train} in Theorem 4 and empirically verify it in Figure 7(a). Since neighbors owning more connections with the whole neighborhood have higher LP scores with the average neighborhood embeddings, we update the adjacency matrix used for message-passing as:

$$\widetilde{\mathbf{A}}_{ij}^{\tau} = \begin{cases} \widetilde{\mathbf{A}}_{ij}^{\tau-1} + \gamma \frac{\exp(g_{\mathbf{\Theta}_g}(\mathbf{N}_i^{\tau-1}, \mathbf{H}_j^{\tau-1}))}{\sum_{j=1}^{n}\exp(g_{\mathbf{\Theta}_g}(\mathbf{N}_i^{\tau-1}, \mathbf{H}_j^{\tau-1}))}, & \text{if} \mathbf{A}_{ij} = 1 \\ 0, & \text{if} \mathbf{A}_{ij} = 0 \end{cases}, \forall v_i, v_j \in \mathcal{V}, \tag{4}$$

where $\mathbf{H}^{\tau-1} = f_{\mathbf{\Theta}_f}(\widetilde{\mathbf{A}}^{\tau-1}, \mathbf{X})$ is the node embeddings obtained from GNN model $f_{\mathbf{\Theta}_f}$, $\mathbf{N}^{\tau-1} = \widetilde{\mathbf{A}}\mathbf{H}^{\tau-1}$ is the average neighborhood embeddings by performing one more SAGE-style propagation, γ is the weight coefficient, $\widetilde{\mathbf{A}}^0 = \widetilde{\mathbf{A}}$, and g_{Θ_g} is the link predictor. The detailed algorithm is presented in Appendix H. Note that this edge reweighting strategy directly operates on the original adjacency matrix and hence shares the same time/space complexity as the conventional message-passing $\mathcal{O}(Ld(|\mathcal{E} + \mathcal{V}|))$ with L being the number of message-passing layers. For baselines obtaining node embeddings without using message-passing such as BUDDY Chamberlain et al. (2022), we reweigh edges in computing the binary cross entropy loss in the training stage. More details are attached Appendix I. Specifically, we equip four baselines, GCN/SAGE/NCN/BUDDY, with our designed edge reweighting strategy and present their LP performance in Table 11. Appendix F thoroughly describes the experimental settings. For GCN, SAGE and BUDDY, equipping with our proposed edge reweighting strategy enhances their LP performance in most cases. This demonstrates that by pushing up the TC^{Train} of the whole graph, the LP performance can be boosted to a certain level, which is also verified by the increasing TC shown in Figure 7(a). We hypothesize that neighbors

Table 1: Results on LP benchmarks. X_{rw} denotes weighted message-passing added to baseline X.

Baseline	Cora Hits@100	Citeseer Hits@100	Pubmed Hits@100	Collab Hits@50	Collab* Hits@50	Citation2 MRR	Reptile Hits@100	Vole Hits@100
GCN	70.63±0.67	65.96±2.12	69.35±1.02	49.52±0.52	58.00±0.27	84.42±0.05	65.52±2.73	73.84±0.98
GCN$_{rw}$	75.98±1.28	74.40±1.13	68.87±0.99	52.85±0.14	60.57±0.38	85.34±0.30	70.79±2.00	74.50±0.84
SAGE	74.27±2.08	61.57±3.28	66.25±1.08	50.01±0.50	57.06±0.06	80.44±0.10	72.59±3.19	80.55±1.59
SAGE$_{rw}$	74.62±2.30	69.89±1.66	66.77±0.69	52.59±0.37	59.26±0.08	80.61±0.10	74.35±3.20	81.27±0.96
NCN	87.73±1.41	90.93±0.83	76.20±1.55	54.43±0.17	65.34±0.03	88.64±0.14	68.37±3.57	66.10±1.13
NCN$_{rw}$	87.95±1.30	91.86±0.82	76.51±1.41	54.16±0.24	65.41±0.03	OOM	73.81±4.71	67.32±0.81
BUDDY	84.82±1.93	91.44±1.14	74.46±3.32	55.73±0.16	66.25±0.28	88.41±0.10	74.69±7.55	83.37±1.05
BUDDY$_{rw}$	85.06±1.81	91.86±1.00	75.74±2.03	56.17±0.42	66.31±0.50	88.48±0.09	77.20±4.10	84.64±1.29

Note that for Citation2, due to memory limitation, we directly take the result from the original NCN paper (Wang et al., 2023). Different from Collab only using training edges in message-passing for evaluating testing performance, we also allow validation edges in Collab*.

connecting more to the overall neighborhood likely have greater interactions with incoming neighbors. Thus, aggregating more information from them inherently captures the common neighbor signals of these incoming neighbors. Meanwhile, as NCN already explicitly accounts for this common neighbor signal in its decoder, the performance gains from our strategy are relatively modest. Furthermore, the positive trend observed in Figure 7(b) verifies that the larger enhancement in node TC^{Train} leads to a larger performance boost in its $\text{Hits}^N@10$. However, we note that LP performance is evaluated on the incoming testing neighbors rather than training neighbors, so TC^{Train} is more of a correlated metric than causal. To illustrate, consider an extreme case where a node v_i has training neighbors forming a complete graph with no connection to its incoming neighbors. In such a scenario, even if we achieve the maximum $\text{TC}^{\text{Train}} = 1$ and a significantly high training performance, it still hardly generalizes to predicting testing links. This could be reflected in the inconsistent trend in Figure 21/22 in Appendix G.7. In addition, Figure 7(c) verifies the assumption made in Theorem 4 and in the reweighting model design that nodes with larger TC^{Train} have higher average embedding similarity to their neighbors.

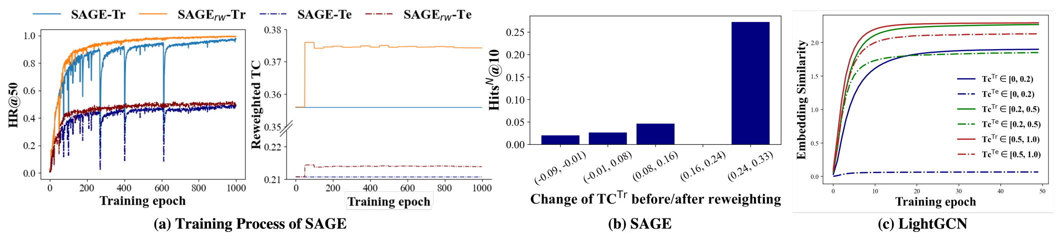

Figure 7: **(a)** Change of Hits@50 and Reweighted TC along the training process in SAGE. **(b)** Nodes with enhanced TC^{Train} exhibit higher performance. **(c)** Embedding similarity during LightGCN training increases faster and higher for nodes with higher TC^{Train}.

5 Conclusion

Although many recent works have achieved unprecedented success in enhancing link prediction (LP) performance with GNNs, demystifying the varying levels of embedding quality and LP performance across different nodes within the graph is heavily under-explored yet fundamental. In this work, we take the lead in understanding the nodes' varying performance from the perspective of their local topology. Given the connection between link formation and the subgraph interaction, we propose Topological Concentration (TC) and demonstrate its superiority in characterizing node LP performance and identifying low-performing nodes by specifically verifying its higher performance correlation than other node-centric topological metrics. Moreover, we discover a novel topological distribution shift (TDS) issue by observing the changing LP performance over time and demonstrate the capability of using TC to measure this distribution shift. Our work offers the community strong insights into which local topology enables nodes to have better LP performance with GNNs. In the future, we plan to investigate the causal relationship between TC and LP. Additionally, we aim to utilize TC for data valuation to select consistently crucial edges in dynamic link prediction.

Acknowledgements

This research is supported by the National Science Foundation (NSF) under grant number IIS2239881 and by Snap Inc.

REFERENCES

Sergey Brin and Lawrence Page. The anatomy of a large-scale hypertextual web search engine. *Computer networks and ISDN systems*, 30(1-7):107–117, 1998.

Benjamin Paul Chamberlain, Sergey Shirobokov, Emanuele Rossi, Fabrizio Frasca, Thomas Markovich, Nils Hammerla, Michael M Bronstein, and Max Hansmire. Graph neural networks for link prediction with subgraph sketching. *arXiv preprint arXiv:2209.15486*, 2022.

Deli Chen, Yankai Lin, Guangxiang Zhao, Xuancheng Ren, Peng Li, Jie Zhou, and Xu Sun. Topology-imbalance learning for semi-supervised node classification. *Advances in Neural Information Processing Systems*, 34:29885–29897, 2021a.

Haochen Chen, Syed Fahad Sultan, Yingtao Tian, Muhao Chen, and Steven Skiena. Fast and accurate network embeddings via very sparse random projection. In *Proceedings of the 28th ACM international conference on information and knowledge management*, pp. 399–408, 2019.

Huiyuan Chen, Lan Wang, Yusan Lin, Chin-Chia Michael Yeh, Fei Wang, and Hao Yang. Structured graph convolutional networks with stochastic masks for recommender systems. In *Proceedings of the 44th International ACM SIGIR Conference on Research and Development in Information Retrieval*, pp. 614–623, 2021b.

Manqing Dong, Feng Yuan, Lina Yao, Xiwei Xu, and Liming Zhu. Mamo: Memory-augmented meta-optimization for cold-start recommendation. In *Proceedings of the 26th ACM SIGKDD international conference on knowledge discovery & data mining*, pp. 688–697, 2020.

Wenqi Fan, Yao Ma, Qing Li, Yuan He, Eric Zhao, Jiliang Tang, and Dawei Yin. Graph neural networks for social recommendation. In *The world wide web conference*, pp. 417–426, 2019.

Hao-Ming Fu, Patrick Poirson, Kwot Sin Lee, and Chen Wang. Revisiting neighborhood-based link prediction for collaborative filtering. In *Companion Proceedings of the Web Conference 2022*, pp. 1009–1018, 2022.

Johannes Gasteiger, Stefan Weißenberger, and Stephan Günnemann. Diffusion improves graph learning. *Advances in neural information processing systems*, 32, 2019.

Liang Ge and Aidong Zhang. Pseudo cold start link prediction with multiple sources in social networks. In *Proceedings of the 2012 SIAM International Conference on Data Mining*, pp. 768–779. SIAM, 2012.

Marco Gori, Augusto Pucci, V Roma, and I Siena. Itemrank: A random-walk based scoring algorithm for recommender engines. In *IJCAI*, volume 7, pp. 2766–2771, 2007.

Aditya Grover and Jure Leskovec. node2vec: Scalable feature learning for networks. In *Proceedings of the 22nd ACM SIGKDD international conference on Knowledge discovery and data mining*, pp. 855–864, 2016.

Zhichun Guo, Tong Zhao, Yozen Liu, Kaiwen Dong, William Shiao, Neil Shah, and Nitesh V Chawla. Node duplication improves cold-start link prediction. *arXiv preprint arXiv:2402.09711*, 2024.

Will Hamilton, Zhitao Ying, and Jure Leskovec. Inductive representation learning on large graphs. *Advances in neural information processing systems*, 30, 2017.

Haoyu Han, Xiaorui Liu, Li Ma, MohamadAli Torkamani, Hui Liu, Jiliang Tang, and Makoto Yamada. Structural fairness-aware active learning for graph neural networks. In *The Twelfth International Conference on Learning Representations*, 2023.

Xiao Han, Leye Wang, Son N Han, Chao Chen, Noël Crespi, and Reza Farahbakhsh. Link prediction for new users in social networks. In *2015 IEEE International Conference on Communications (ICC)*, pp. 1250–1255. IEEE, 2015.

Bowen Hao, Jing Zhang, Hongzhi Yin, Cuiping Li, and Hong Chen. Pre-training graph neural networks for cold-start users and items representation. In *Proceedings of the 14th ACM International Conference on Web Search and Data Mining*, pp. 265–273, 2021.

Xiangnan He, Kuan Deng, Xiang Wang, Yan Li, Yongdong Zhang, and Meng Wang. Lightgcn: Simplifying and powering graph convolution network for recommendation. In *Proceedings of the 43rd International ACM SIGIR conference on research and development in Information Retrieval*, pp. 639–648, 2020.

Weihua Hu, Matthias Fey, Marinka Zitnik, Yuxiao Dong, Hongyu Ren, Bowen Liu, Michele Catasta, and Jure Leskovec. Open graph benchmark: Datasets for machine learning on graphs. *Advances in neural information processing systems*, 33:22118–22133, 2020.

Thomas N Kipf and Max Welling. Semi-supervised classification with graph convolutional networks. *arXiv preprint arXiv:1609.02907*, 2016.

Sang Gyu Kwak and Jong Hae Kim. Central limit theorem: the cornerstone of modern statistics. *Korean journal of anesthesiology*, 70(2):144–156, 2017.

Vincent Leroy, B Barla Cambazoglu, and Francesco Bonchi. Cold start link prediction. In *Proceedings of the 16th ACM SIGKDD international conference on Knowledge discovery and data mining*, pp. 393–402, 2010.

Juanhui Li, Harry Shomer, Haitao Mao, Shenglai Zeng, Yao Ma, Neil Shah, Jiliang Tang, and Dawei Yin. Evaluating graph neural networks for link prediction: Current pitfalls and new benchmarking. *arXiv preprint arXiv:2306.10453*, 2023.

Yunqi Li, Hanxiong Chen, Zuohui Fu, Yingqiang Ge, and Yongfeng Zhang. User-oriented fairness in recommendation. In *Proceedings of the Web Conference 2021*, pp. 624–632, 2021.

David Liben-Nowell and Jon Kleinberg. The link prediction problem for social networks. In *Proceedings of the twelfth international conference on Information and knowledge management*, pp. 556–559, 2003.

Blerina Lika, Kostas Kolomvatsos, and Stathes Hadjiefthymiades. Facing the cold start problem in recommender systems. *Expert systems with applications*, 41(4):2065–2073, 2014.

Zemin Liu, Trung-Kien Nguyen, and Yuan Fang. Tail-gnn: Tail-node graph neural networks. In *Proceedings of the 27th ACM SIGKDD Conference on Knowledge Discovery & Data Mining*, pp. 1109–1119, 2021.

Yao Ma, Ziyi Guo, Zhaocun Ren, Jiliang Tang, and Dawei Yin. Streaming graph neural networks. In *Proceedings of the 43rd international ACM SIGIR conference on research and development in information retrieval*, pp. 719–728, 2020.

Haitao Mao, Zhikai Chen, Wei Jin, Haoyu Han, Yao Ma, Tong Zhao, Neil Shah, and Jiliang Tang. Demystifying structural disparity in graph neural networks: Can one size fit all? *arXiv preprint arXiv:2306.01323*, 2023.

Mark EJ Newman. Clustering and preferential attachment in growing networks. *Physical review E*, 64(2):025102, 2001.

John Palowitch, Anton Tsitsulin, Brandon Mayer, and Bryan Perozzi. Graphworld: Fake graphs bring real insights for gnns. In *Proceedings of the 28th ACM SIGKDD Conference on Knowledge Discovery and Data Mining*, pp. 3691–3701, 2022.

Liming Pan, Cheng Shi, and Ivan Dokmanić. Neural link prediction with walk pooling. In *International Conference on Learning Representations*, 2022.

Joonhyung Park, Jaeyun Song, and Eunho Yang. Graphens: Neighbor-aware ego network synthesis for class-imbalanced node classification. In *International Conference on Learning Representations*, 2021.

Bryan Perozzi, Rami Al-Rfou, and Steven Skiena. Deepwalk: Online learning of social representations. In *Proceedings of the 20th ACM SIGKDD international conference on Knowledge discovery and data mining*, pp. 701–710, 2014.

Hossein A Rahmani, Mohammadmehdi Naghiaei, Mahdi Dehghan, and Mohammad Aliannejadi. Experiments on generalizability of user-oriented fairness in recommender systems. In *Proceedings of the 45th International ACM SIGIR Conference on Research and Development in Information Retrieval*, pp. 2755–2764, 2022.

Emanuele Rossi, Ben Chamberlain, Fabrizio Frasca, Davide Eynard, Federico Monti, and Michael Bronstein. Temporal graph networks for deep learning on dynamic graphs. *arXiv preprint arXiv:2006.10637*, 2020.

Ryan A. Rossi and Nesreen K. Ahmed. The network data repository with interactive graph analytics and visualization. In *AAAI*, 2015. URL `https://networkrepository.com`.

Benedek Rozemberczki, Charles Tapley Hoyt, Anna Gogleva, Piotr Grabowski, Klas Karis, Andrej Lamov, Andriy Nikolov, Sebastian Nilsson, Michael Ughetto, Yu Wang, Tyler Derr, and Benjamin M. Gyori. Chemicalx: A deep learning library for drug pair scoring. In *Proceedings of the 28th ACM SIGKDD Conference on Knowledge Discovery and Data Mining*, pp. 3819–3828, 2022.

MN Sanders. Characteristic function of the central chi-squared distribution, 2009.

Hibiki Taguchi, Xin Liu, and Tsuyoshi Murata. Graph convolutional networks for graphs containing missing features. *Future Generation Computer Systems*, 117:155–168, 2021.

Qiaoyu Tan, Xin Zhang, Ninghao Liu, Daochen Zha, Li Li, Rui Chen, Soo-Hyun Choi, and Xia Hu. Bring your own view: Graph neural networks for link prediction with personalized subgraph selection. In *Proceedings of the Sixteenth ACM International Conference on Web Search and Data Mining*, pp. 625–633, 2023.

Xianfeng Tang, Huaxiu Yao, Yiwei Sun, Yiqi Wang, Jiliang Tang, Charu Aggarwal, Prasenjit Mitra, and Suhang Wang. Investigating and mitigating degree-related biases in graph convoltuional networks. In *Proceedings of the 29th ACM International Conference on Information & Knowledge Management*, pp. 1435–1444, 2020.

Hongwei Wang, Fuzheng Zhang, Miao Zhao, Wenjie Li, Xing Xie, and Minyi Guo. Multi-task feature learning for knowledge graph enhanced recommendation. In *The world wide web conference*, pp. 2000–2010, 2019.

Ruijia Wang, Xiao Wang, Chuan Shi, and Le Song. Uncovering the structural fairness in graph contrastive learning. *Advances in Neural Information Processing Systems*, 35:32465–32473, 2022a.

Xiyuan Wang, Haotong Yang, and Muhan Zhang. Neural common neighbor with completion for link prediction. *arXiv preprint arXiv:2302.00890*, 2023.

Yiwei Wang, Wei Wang, Yuxuan Liang, Yujun Cai, and Bryan Hooi. Mixup for node and graph classification. In *Proceedings of the Web Conference 2021*, pp. 3663–3674, 2021.

Yu Wang and Tyler Derr. Degree-related bias in link prediction. In *2022 IEEE International Conference on Data Mining Workshops (ICDMW)*, pp. 757–758. IEEE, 2022.

Yu Wang, Yuying Zhao, Neil Shah, and Tyler Derr. Imbalanced graph classification via graph-of-graph neural networks. In *Proceedings of the 31st ACM International Conference on Information & Knowledge Management*, pp. 2067–2076, 2022b.

Yu Wang, Yuying Zhao, Yi Zhang, and Tyler Derr. Collaboration-aware graph convolutional networks for recommendation systems. *arXiv preprint arXiv:2207.06221*, 2022c.

Zhiqiang Wang, Jiye Liang, Ru Li, and Yuhua Qian. An approach to cold-start link prediction: Establishing connections between non-topological and topological information. *IEEE Transactions on Knowledge and Data Engineering*, 28(11):2857–2870, 2016.

Tianxin Wei and Jingrui He. Comprehensive fair meta-learned recommender system. In *Proceedings of the 28th ACM SIGKDD Conference on Knowledge Discovery and Data Mining*, pp. 1989–1999, 2022.

Linchuan Xu, Xiaokai Wei, Jiannong Cao, and Philip S Yu. On learning mixed community-specific similarity metrics for cold-start link prediction. In *Proceedings of the 26th International Conference on World Wide Web Companion*, pp. 861–862, 2017.

Ming Yan, Jitao Sang, Tao Mei, and Changsheng Xu. Friend transfer: Cold-start friend recommendation with cross-platform transfer learning of social knowledge. In *2013 IEEE International Conference on Multimedia and Expo (ICME)*, pp. 1–6. IEEE, 2013.

Haoteng Yin, Muhan Zhang, Yanbang Wang, Jianguo Wang, and Pan Li. Algorithm and system co-design for efficient subgraph-based graph representation learning. *arXiv preprint arXiv:2202.13538*, 2022.

Rex Ying, Ruining He, Kaifeng Chen, Pong Eksombatchai, William L Hamilton, and Jure Leskovec. Graph convolutional neural networks for web-scale recommender systems. In *Proceedings of the 24th ACM SIGKDD international conference on knowledge discovery & data mining*, pp. 974–983, 2018.

Seongjun Yun, Seoyoon Kim, Junhyun Lee, Jaewoo Kang, and Hyunwoo J Kim. Neo-gnns: Neighborhood overlap-aware graph neural networks for link prediction. *Advances in Neural Information Processing Systems*, 34:13683–13694, 2021.

Muhan Zhang and Yixin Chen. Link prediction based on graph neural networks. *Advances in neural information processing systems*, 31, 2018.

Tianxiang Zhao, Xiang Zhang, and Suhang Wang. Graphsmote: Imbalanced node classification on graphs with graph neural networks. In *Proceedings of the 14th ACM international conference on web search and data mining*, pp. 833–841, 2021a.

Tong Zhao, Yozen Liu, Leonardo Neves, Oliver Woodford, Meng Jiang, and Neil Shah. Data augmentation for graph neural networks. In *Proceedings of the aaai conference on artificial intelligence*, volume 35, pp. 11015–11023, 2021b.

Tong Zhao, Gang Liu, Daheng Wang, Wenhao Yu, and Meng Jiang. Learning from counterfactual links for link prediction. In *International Conference on Machine Learning*, pp. 26911–26926. PMLR, 2022.

Xiangyu Zhao, Haochen Liu, Wenqi Fan, Hui Liu, Jiliang Tang, Chong Wang, Ming Chen, Xudong Zheng, Xiaobing Liu, and Xiwang Yang. Autoemb: Automated embedding dimensionality search in streaming recommendations. In *2021 IEEE International Conference on Data Mining (ICDM)*, pp. 896–905. IEEE, 2021c.

Xiangyu Zhao, Haochen Liu, Hui Liu, Jiliang Tang, Weiwei Guo, Jun Shi, Sida Wang, Huiji Gao, and Bo Long. Autodim: Field-aware embedding dimension searchin recommender systems. In *Proceedings of the Web Conference 2021*, pp. 3015–3022, 2021d.

Yuying Zhao, Yu Wang, Yunchao Liu, Xueqi Cheng, Charu Aggarwal, and Tyler Derr. Fairness and diversity in recommender systems: a survey. *arXiv preprint arXiv:2307.04644*, 2023.

Yuying Zhao, Minghua Xu, Huiyuan Chen, Yuzhong Chen, Yiwei Cai, Rashidul Islam, Yu Wang, and Tyler Derr. Can one embedding fit all? a multi-interest learning paradigm towards improving user interest diversity fairness. *arXiv preprint arXiv:2402.13495*, 2024.

Jiong Zhu, Yujun Yan, Lingxiao Zhao, Mark Heimann, Leman Akoglu, and Danai Koutra. Beyond homophily in graph neural networks: Current limitations and effective designs. *Advances in Neural Information Processing Systems*, 33:7793–7804, 2020.

Jiong Zhu, Ryan A Rossi, Anup Rao, Tung Mai, Nedim Lipka, Nesreen K Ahmed, and Danai Koutra. Graph neural networks with heterophily. In *Proceedings of the AAAI conference on artificial intelligence*, volume 35, pp. 11168–11176, 2021.

Appendix

Table of Contents

A Notations

This section summarizes notations used throughout this paper.

Table 2: Notations used throughout this paper.

Notations	**Definitions or Descriptions**
$G = (\mathcal{V}, \mathcal{E}, \mathbf{X})$	Graph with node set $\mathcal{V}$, edge set $\mathcal{E}$ and node feature $\mathbf{X}$
m, n	Number of nodes $m = \|\mathcal{V}\|$ and number of edges $n = \|\mathcal{E}\|$
v_i, e_{ij}	Node v_i and the edge e_{ij} between node v_i and v_j
$\mathbf{A}$	Adjacency matrix $\mathbf{A}_{ij} = 1$ indicates an edge e_{ij} between v_i, v_j
$\widetilde{\mathbf{A}}$	Row-based normalized graph adjacency matrix $\widetilde{\mathbf{A}} = \mathbf{D}^{-1}\mathbf{A}$
$\widehat{\mathbf{A}}$	GCN-based normalized graph adjacency matrix $\widehat{\mathbf{A}} = \mathbf{D}^{-0.5}\mathbf{A}\mathbf{D}^{-0.5}$
$\widetilde{\mathbf{A}}^t$	Updated adjacency matrix at iteration t
$\mathbf{D}$	Diagonal degree matrix $\mathbf{D}_{ii} = \sum_{j=1}^{n} \mathbf{A}_{ij}$
$\widehat{d}$	Average degree of the network
$\mathcal{T} = \{\text{Train, Val, Test}\}$	Set of Training/Validation/Testing edge groups
$\text{Degree}^{\text{Train/Val/Test}}$	Degree based on Training/Validation/Testing Edges
$\text{TC}^{\text{Train/Val/Test}}$	Topological Concentrations that quantify intersections with Training/Validation/Testing neighbors
$\mathcal{N}_i^t$	Node v_i's 1-hop neighbors of type $t, t \in \mathcal{T}$
$\mathcal{H}_i^k$	Nodes having at least one path of length k to v_i based on training edges $\mathcal{E}^{\text{Train}}$
$\mathcal{S}_i^K = \{\mathcal{H}_i^k\}_{k=1}^K$	K-hop computational tree centered on the node v_i
$C_i^{K,t} \backslash \widetilde{C}_i^{K,t}$	(Approximated) Topological concentration for node v_i considering the intersection among K-hop computational trees among its type t neighbors.
$\mathbf{E}_i^k$	Embedding of the node v_i after k^{th}-layer message-passing
$\mathbf{R}_{ij}$	Sample from gaussian random variable $\mathcal{N}(0, 1/d)$
$g_{\mathbf{\Theta}_g}$	Link predictor parameterized by $\mathbf{\Theta}_g$
$\widetilde{\mathcal{E}}_i, \widehat{\mathcal{E}}_i$	Predicted and ground-truth neighbors of node v_i
$\mathcal{HG}$	Hypergeometric distribution
LP	Link Prediction
(A)TC	(Approxminated) Topological Concentration
TDS	Topological Distribution Shift
β	Exponential discounting effect as the hop increases
α_k	Weighted coefficient of layer k in computing ATC
μ	Mean of the distribution
L	Number of message-passing layers
γ	Coefficients measuring the contribution of updating adjacency matrix

B Review of the cold-start issue in link prediction and recommender systems

One line of the research (Leroy et al., 2010; Ge & Zhang, 2012; Yan et al., 2013; Han et al., 2015; Wang et al., 2016; Xu et al., 2017) defines the cold-start nodes as the ones with little to no topological information (isolated user) and augment these disadvantaged groups with auxiliary information, e.g., user profile/rich text information, community information, and group membership. Specifically, (Yan et al., 2013) derive the auxiliary information based on the interactions of these disadvantageous nodes/users from their cross-platform behaviors. (Leroy et al., 2010) constructs the probabilistic graph and then refines it by considering the transitivity of the contract relationship. (Ge & Zhang, 2012) incorporates feature selection and regularization to avoid overfitting. The other line of research (Wang et al., 2019; Dong et al., 2020; Li et al., 2021; Hao et al., 2021; Rahmani et al., 2022; Wei & He, 2022) studies the cold-start issue from the user perspective in recommender systems. They usually define cold-start nodes/users as the ones with no-to-sparse/low activities. (Li et al., 2021; Rahmani et al., 2022) devises a re-ranking strategy by optimizing the performance gap between low-activity and high-activity users. (Dong et al., 2020; Wei & He, 2022) design multiple meta-learning frameworks to learn user preferences based on his/her few past interactions. (Wang et al., 2019) uses knowledge graph embedding to assist with recommendation tasks for low-activity users while (Hao et al., 2021) trains GNNs to adapt to cold-start nodes by mimicking the cold-start scenario for warm users.

Following the above second line of research, we study the cold-start link prediction at the node level since our paper targets demystifying the varying link prediction performance across different nodes. Therefore, we follow some conventional literature (Wang et al., 2019; Dong et al., 2020; Li et al., 2021; Wei & He, 2022) and deem the nodes with generally few degrees as cold-start ones. Particularly, in Figure 4(b)/(e), we change the degree threshold from 1 to 10, divide nodes into two groups at each degree threshold, and further visualize the average performance for each group. We can see that nodes in the lower-degree groups generally have higher performance than nodes in the higher-degree groups. The above observation has two promising insights compared with conventional literature:

- **(1)** Many existing recommendation-based papers (Wang et al., 2019; Dong et al., 2020; Li et al., 2021; Newman, 2001) define cold-start users/nodes as the ones with few/little interactions/topological signals. However, our paper empirically demonstrates that nodes with lower degrees even exhibit higher LP performance.
- **(2)** Many existing node classification papers (Tang et al., 2020; Chen et al., 2021a; Wang et al., 2022a) find nodes with low degrees have lower performance. However, our work sheds new insights into the degree-related bias in link prediction where nodes with lower degrees can actually possess higher performance.

We justify the above 1^{st} insight by relating to real-world scenarios where users with high degrees usually tend to possess diverse interests (nodes with higher degrees may tend to belong to diverse communities) and therefore, using the equal capacity of embedding cannot equally characterize all of their interests (Zhao et al., 2021d).

We justify the above 2^{nd} insight by relating to the inherent difference between the mechanism of node classification and the mechanism of link prediction. For node classification, high-degree nodes are more likely to obtain the supervised signals from labeled nodes in the same class (Chen et al., 2021a). For link prediction, the ground-truth class for each node is actually its testing neighbors and hence when performing message-passing, beneficial supervision signals are not guaranteed to be captured more by high-degree nodes.

In our paper, we focus on the performance difference between low-degree nodes and high-degree nodes rather than the cold-start issue. However, if we also consider cold-start nodes as the ones with sparse interactions as some previous work did (Li et al., 2021; Rahmani et al., 2022), then our analysis and observation can also apply there.

C Link-centric and Node-centric Evaluation Metrics

In addition to the conventional link-centric evaluation metrics used in this work, node-centric evaluation metrics are also used to mitigate the positional bias caused by the tiny portion of the sampled negative links. We introduce their mathematical definition respectively as follows:

C.1 Link-Centric Evaluation

Following (Hu et al., 2020), we rank the prediction score of each link among a set of randomly sampled negative node pairs and calculate the link-centric evaluation metric Hits@K as the ratio of positive edges that are ranked at K^{th}-place or above. Note that this evaluation may cause bias as the sampled negative links only count a tiny portion of the quadratic node pairs (Li et al., 2023). Hereafter, we introduce the node-centric evaluation metrics and specifically denote the node-level Hit ratio as Hits^N@K to differentiate it from the link-centric evaluation metric Hits@K.

C.2 Node-Centric Evaluation

For each node $v_i \in \mathcal{V}$, the model predicts the link formation score between v_i and *every other node*, and selects the top-K nodes to form the potential candidates $\widetilde{\mathcal{E}}_i$. Since the ground-truth candidates for node v_i is $\mathcal{N}_i^{\text{Test}}$ (hereafter, we notate as $\widehat{\mathcal{E}}_i$), we can compute the Recall (R), Precision (P), F1, NDCG (N), MRR and Hits^N of v_i as follows:

$$\text{R@}K_i = \frac{|\widetilde{\mathcal{E}}_i \cap \widehat{\mathcal{E}}_i|}{|\widehat{\mathcal{E}}_i|}, \qquad \text{P@}K_i = \frac{|\widetilde{\mathcal{E}}_i \cap \widehat{\mathcal{E}}_i|}{K} \tag{5}$$

$$\text{F1@}K_i = \frac{2|\widetilde{\mathcal{E}}_i \cap \widehat{\mathcal{E}}_i|}{K + |\widehat{\mathcal{E}}_i|}, \qquad \text{N@}K_i = \frac{\sum_{k=1}^{K} \frac{\mathbb{1}[v_{\phi_i^k} \in (\widetilde{\mathcal{E}}_i \cap \widehat{\mathcal{E}}_i)]}{\log_2(k+1)}}{\sum_{k=1}^{K} \frac{1}{\log_2(k+1)}} \tag{6}$$

$$\text{MRR@}K_i = \frac{1}{\min_{v \in (\widetilde{\mathcal{E}}_i \cap \widehat{\mathcal{E}}_i)} \text{Rank}_v}, \qquad \text{Hits}^N\text{@}K_i = \mathbb{1}[|\widehat{\mathcal{E}}_i \cap \widetilde{\mathcal{E}}_i| > 0], \tag{7}$$

where ϕ_i^k denotes v_i's k^{th} preferred node according to the ranking of the link prediction score, Rank$_v$ is the ranking of the node v and $\mathbb{1}$ is the indicator function equating 0 if the intersection between $\widehat{\mathcal{E}}^i \cap \widetilde{\mathcal{E}}_i$ is empty otherwise 1. The final performance of each dataset is averaged across each node:

$$\text{X@}K = \mathbb{E}_{v_i \in \mathcal{V}} X\text{@}K_i, \text{X} \in \{\text{R}, \text{P}, \text{F1}, \text{N}, \text{MRR}, \text{Hits}^N\} \tag{8}$$

Because for each node, the predicted neighbors will be compared against all the other nodes, there is no evaluation bias compared with the link-centric evaluation where only a set of randomly selected negative node pairs are used.

D PROOF OF THEOREMS

D.1 APPROXIMATION POWER OF ATC FOR TC

Theorem 1. *Assuming $g(|\mathcal{H}_i^{k_1}|, |\mathcal{H}_j^{k_2}|) = |\mathcal{H}_i^{k_1}||\mathcal{H}_j^{k_2}|$ in Eq. (1) and let ϕ be the dot-product based similarity metric (He et al., 2020), then node v_i's 1-layer Topological Concentration $C_i^{1,t}$ is linear correlated with the mean value of the 1-layer Approximated Topological Concentration $\mu_{\widetilde{C}_i^{K,t}}$ as:*

$$C_i^{1,t} \approx d^{-1}\mu_{\mathbb{E}_{v_j\sim\mathcal{N}_i^t}(\mathbf{E}_j^1)^\top \mathbf{E}_i^1} = d^{-1}\mu_{\widetilde{C}_i^{1,t}}, \tag{9}$$

where $\mathbf{E}^1 \in \mathbb{R}^{n\times d}$ denotes the node embeddings after 1-layer SAGE-style message-passing over the node embeddings $\mathbf{R} \sim \mathcal{N}(\mathbf{0}^d, \mathbf{\Sigma}^d)$.

Proof. Assuming without loss of generalizability that the row-normalized adjacency matrix $\widetilde{\mathbf{A}} = \mathbf{D}^{-1}\mathbf{A}$ is used in aggregating neighborhood embeddings. We focus on a randomly selected node $\mathbf{E}_i \in \mathbb{R}^d, \forall v_i \in \mathcal{V}$ and its 1-layer ATC given by Eq. (2) is:

$$\begin{aligned}
\widetilde{C}_i^{1,t} = \mathbb{E}_{v_j\sim\mathcal{N}_i^t}(\mathbf{E}_j^1)^\top \mathbf{E}_i^1 &= \mathbb{E}_{v_j\sim\mathcal{N}_i^t}(\widetilde{\mathbf{A}}\mathbf{R})_j^\top(\widetilde{\mathbf{A}}\mathbf{R})_i \\
&= \mathbb{E}_{v_j\sim\mathcal{N}_i^t}\frac{1}{|\mathcal{N}_j^{\text{Train}}||\mathcal{N}_i^{\text{Train}}|}\Big(\sum_{v_m\in\mathcal{N}_j^{\text{Train}}}\mathbf{R}_m\Big)^\top\Big(\sum_{v_n\in\mathcal{N}_i^{\text{Train}}}\mathbf{R}_n\Big) \\
&= \mathbb{E}_{v_j\sim\mathcal{N}_i^t}\frac{1}{|\mathcal{N}_j^{\text{Train}}||\mathcal{N}_i^{\text{Train}}|}\sum_{(v_m,v_n)\in\mathcal{N}_j^{\text{Train}}\times\mathcal{N}_i^{\text{Train}}}(\mathbf{R}_m)^\top\mathbf{R}_n \\
&= \mathbb{E}_{v_j\sim\mathcal{N}_i^t}\frac{1}{|\mathcal{H}_i^1||\mathcal{H}_j^1|}\Big(\underbrace{\sum_{\substack{(v_m,v_n)\in\mathcal{N}_j^{\text{Train}}\times\mathcal{N}_i^{\text{Train}},\\ v_m\neq v_n}}(\mathbf{R}_m)^\top\mathbf{R}_n}_{\text{Non-common neighbor embedding pairs}} + \underbrace{\sum_{v_k\in\mathcal{N}_j^{\text{Train}}\cap\mathcal{N}_i^{\text{Train}}}(\mathbf{R}_k)^\top\mathbf{R}_k}_{\text{Common neighbor embedding pairs}}\Big),
\end{aligned} \tag{10}$$

Note that the first term is the dot product between any pair of two non-common neighbor embeddings, which is essentially the dot product between two independent samples from the same multivariate Gaussian distribution (*note that here we do not perform any training optimization, so the embeddings of different nodes are completely independent*). By central limit theorem (Kwak & Kim, 2017), the first term approaches the standard Gaussian distribution with 0 as the mean, $i.e., \mu_{(\mathbf{R}_m)^\top\mathbf{R}_n} = 0$. In contrast, the second term is the dot product between any Gaussian-distributed sample and itself, which can be essentially characterized as the sum of squares of d independent standard normal random variables and hence follows the chi-squared distribution with d degrees of freedom, i.e., $(\mathbf{R}_k)^\top\mathbf{R}_k \sim \chi_d^2$ (Sanders, 2009). By Central Limit Theorem, $\lim_{d\to\infty} P(\frac{\chi_d^2 - d}{\sqrt{2d}} \leq z) = P_{\mathcal{N}(0,1)}(z)$ and hence $\lim_{d\to\infty}\chi_d^2 = \mathcal{N}(d, 2d), i.e., \mu_{(\mathbf{R}_k)^\top\mathbf{R}_k} = d$. Then we obtain the mean value of $\mathbb{E}_{v_j\sim\mathcal{N}_i^t}(\mathbf{E}_j^1)^\top\mathbf{E}_i^1$:

$$\begin{aligned}
\mu_{\widetilde{C}_i^{1,t}} = \mu_{\mathbb{E}_{v_j\sim\mathcal{N}_i^t}(\mathbf{E}_j^1)^\top\mathbf{E}_i^1} &\approx \mathbb{E}_{v_j\sim\mathcal{N}_i^t}\frac{1}{|\mathcal{H}_i^1||\mathcal{H}_j^1|}\Big(\mu_{\sum_{\substack{(v_m,v_n)\in\mathcal{N}_j^{\text{Train}}\times\mathcal{N}_i^{\text{Train}},\\ v_m\neq v_n}}(\mathbf{R}_m)^\top\mathbf{R}_n} + \mu_{\sum_{v_k\in\mathcal{N}_j^{\text{Train}}\cap\mathcal{N}_i^{\text{Train}}}(\mathbf{R}_k)^\top\mathbf{R}_k}\Big) \\
&\approx \mathbb{E}_{v_j\in\mathcal{N}_i^t}\frac{d|\mathcal{N}_i^{\text{Train}}\cap\mathcal{N}_j^{\text{Train}}|}{|\mathcal{H}_i^1||\mathcal{H}_j^1|} = \mathbb{E}_{v_j\in\mathcal{N}_i^t}\frac{d|\mathcal{H}_i^1\cap\mathcal{H}_j^1|}{|\mathcal{H}_i^1||\mathcal{H}_j^1|} = dC_i^{1,t}.
\end{aligned} \tag{11}$$

The first approximation holds if assuming all nodes share the same degree. The second approximation holds since we set d to be at least 64 for all experiments in this paper. We next perform Monte-Carlo Simulation to verify that by setting $d = 64$, the obtained distribution is very similar to the Gaussian distribution. Assuming without loss of generality that the embedding dimension is 64 with the mean vector $\boldsymbol{\mu} = \mathbf{0}^{64} \in \mathbb{R}^{64}$ and the identity covariance matrix $\mathbf{\Sigma}^{64} = \mathbf{I} \in \mathbb{R}^{64\times 64}$, we randomly sample 1000 embeddings from $\mathcal{N}(\boldsymbol{\mu}, \mathbf{\Sigma})$.

We visualize the distributions of the inner product between the pair of non-common neighbor embeddings, i.e., the first term in Eq. (10) $(\mathbf{R}_m)^\top\mathbf{R}_n, v_m \neq v_n$, and the pair of common neighbor embeddings, i.e., the second term in Eq. (10) $(\mathbf{R}_k)^\top\mathbf{R}_k, v_k \in \mathcal{N}_j^{\text{Train}} \cap \mathcal{N}_i^{\text{Train}}$ in Figure 8. We can see that the distribution of the dot product between the pair of non-common neighbor embeddings behaves like a Gaussian distribution centering around 0. In contrast, the distribution of the dot product between the pair of common neighbor embeddings behaves like a chi-square distribution of degree 64, which also centers around 64, and this in turn verifies the Gaussian approximation. Note that the correctness of the first approximation in Eq. (11) relies on the assumption that the average of the inverse of the node's neighbors should be the same across all nodes. Although it cannot be theoretically satisfied, we still empirically verify the positive correlation between TC and the link prediction performance shown in Figure 3.

The above derivation bridges the gap between the Topological Concentration (TC) defined in the topological space and the Approximated Topological Concentration (ATC) defined in the latent space, which theoretically justifies the approximation efficacy of ATC. □

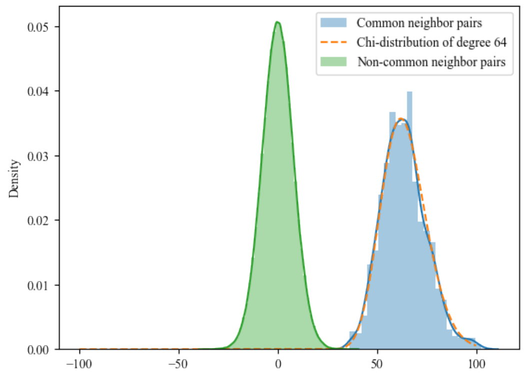

Figure 8: The distribution of the inner product between common neighbor pairs is statistically higher than that between non-common neighbor pairs.

D.2 Degree-related Bias of Evaluation Metrics

One previous work (Wang & Derr, 2022) has empirically shown the degree-related bias of evaluation metrics used in link prediction models. Following that, we go one step further and theoretically derive the concrete format of the evaluation bias in this section. We leverage an untrained link prediction model to study the bias. This avoids any potential supervision signal from training over observed links and enables us to study the evaluation bias exclusively. Since two nodes with the same degree may end up with different performances, i.e., $\text{X@}K_i \neq \text{X@}K_j, d_i = d_j$, we model $\text{X@}K|d$ as a random variable and expect to find the relationship between its expectation and the node degree d, i.e., $f: E(\text{X@}K|d) = f(d)$.

Following many existing ranking works (He et al., 2020; Chen et al., 2021b), we assume without loss of generalizability that the link predictor $\mathscr{P}$ ranking the predicted neighbors based on their embedding similarity with embeddings noted as $\mathbf{E}$, then we have:

Lemma 1. *For any untrained embedding-based link predictor $\mathscr{P}$, given the existing $k-1$ predicted neighbors for the node $v_i \in \mathcal{V}$, the k^{th} predicted neighbor is generated by randomly selecting a node without replacement from the remaining nodes with equal opportunities, i.e., $P(v_{\phi_i^k} = v|\{v_{\phi_i^1}, v_{\phi_i^2}, ..., v_{\phi_i^{k-1}}\}) = \frac{1}{N-(k-1)}$.*

Without any training, Lemma 1 trivially holds since embeddings of all nodes are the same, which trivially leads to the following theorem:

Theorem 2. *Given the untrained embedding-based link predictor $\mathscr{P}$, the size of the intersection between any node's predicted list $\widetilde{\mathcal{E}}_i$ and its ground-truth list $\widehat{\mathcal{E}}_i$ follows a hypergeometric distribution: $|\widetilde{\mathcal{E}}_i \cap \widehat{\mathcal{E}}_i| \sim \mathcal{HG}(|\mathcal{V}|, K, |\widehat{\mathcal{E}}_i|)$ where $|\mathcal{V}|$ is the population size (the whole node space), K is* *the number of trials and $|\widehat{\mathcal{E}}_i|$ is the number of successful states (the number of node's ground-truth neighbors).*

Proof. Given the ground-truth node neighbors $\widehat{\mathcal{E}}_i$, the predicted neighbors $\widetilde{\mathcal{E}}_i = \{v_{\phi_i^k}\}_{k=1}^K$ is formed by selecting one node at a time without replacement K times from the whole node space $\mathcal{V}$. Since any selected node $v_{\phi_i^k}$ can be classified into one of two mutually exclusive categories $\widehat{\mathcal{E}}_i$ or $\mathcal{V}\backslash\widehat{\mathcal{E}}_i$ and by Lemma 1, we know that for any untrained link predictor, each unselected node has an equal opportunity to be selected in every new trial, we conclude that $|\widetilde{\mathcal{E}}_i \cap \widehat{\mathcal{E}}_i| \sim \mathcal{HG}(|\mathcal{V}|, K, |\widehat{\mathcal{E}}_i|)$ and by default $E(|\widetilde{\mathcal{E}}_i \cap \widehat{\mathcal{E}}_i|) = |\widetilde{\mathcal{E}}_i|\frac{|\widehat{\mathcal{E}}_i|}{|\mathcal{V}|} = K\frac{|\widehat{\mathcal{E}}_i|}{|\mathcal{V}|}$. □

Furthermore, we present Theorem 3 to state the relationships between the LP performance under each evaluation metric and the node degree:

Theorem 3. *Given that $|\widetilde{\mathcal{E}}_i \cap \widehat{\mathcal{E}}_i|$ follows hyper-geometric distribution, we have:*

$$E(\text{R@}K_i|d) = \frac{K}{N}, \frac{\partial E(\text{R@}K|d)}{\partial d} = 0, \tag{12}$$

$$E(\text{P@}K|d_i) = \frac{\alpha d}{N}, \frac{\partial E(\text{P@}K|d)}{\partial d} = \frac{\alpha}{N}, \tag{13}$$

$$E(\text{F1@}K|d) = \frac{2K}{N}\frac{\alpha d}{K+\alpha d}, \frac{\partial E(\text{F1@}K|d)}{\partial d} = \frac{2\alpha K^2}{N}\frac{1}{(K+\alpha d)^2}, \tag{14}$$

$$E(\text{N@}K|d) = \frac{\alpha d}{N}, \frac{\partial E(\text{N@}K|d)}{\partial d} = \frac{\alpha}{N}. \tag{15}$$

Proof.

$$E(\text{R@}K_i|d) = E(\frac{|\widetilde{\mathcal{E}}_i \cap \widehat{\mathcal{E}}_i|}{|\widehat{\mathcal{E}}_i|}) = \frac{E(|\widetilde{\mathcal{E}}_i \cap \widehat{\mathcal{E}}_i|)}{|\widehat{\mathcal{E}}_i|} = \frac{\frac{|\widehat{\mathcal{E}}_i|}{|\mathcal{V}|}K}{|\widehat{\mathcal{E}}_i|} = \frac{K}{N} \tag{16}$$

$$E(\text{P@}K_i|d) = E(\frac{|\widetilde{\mathcal{E}}_i \cap \widehat{\mathcal{E}}_i|}{K}) = \frac{E(|\widetilde{\mathcal{E}}_i \cap \widehat{\mathcal{E}}_i|)}{K} = \frac{\frac{|\widehat{\mathcal{E}}_i|}{|\mathcal{V}|}K}{K} = \frac{\alpha d}{N} \tag{17}$$

$$E(\text{F1@}K_i|d) = E(\frac{2|\widetilde{\mathcal{E}}_i \cap \widehat{\mathcal{E}}_i|}{K+|\widehat{\mathcal{E}}_i|}) = \frac{2E(|\widetilde{\mathcal{E}}_i \cap \widehat{\mathcal{E}}_i|)}{K+\alpha d} = \frac{2K}{N}\frac{\alpha d}{K+\alpha d} \tag{18}$$

$$E(\text{N@}K_i|d) = E(\frac{\sum_{k=1}^K \frac{\mathbb{1}[v_{\phi^k} \in (\widetilde{\mathcal{E}}_i \cap \widehat{\mathcal{E}}_i)]}{\log_2(k+1)}}{\sum_{k=1}^K \log_2(k+1)}) = \frac{E(\sum_{k=1}^K \frac{\mathbb{1}[v_{\phi^k} \in (\widetilde{\mathcal{E}}_i \cap \widehat{\mathcal{E}}_i)]}{\log_2(k+1)})}{\sum_{k=1}^K \frac{1}{\log_2(k+1)}} \tag{19}$$

To calculate the numerator DCG, i.e., $E(\sum_{k=1}^K \frac{\mathbb{1}[v_{\phi^k} \in (\widetilde{\mathcal{E}}_i \cap \widehat{\mathcal{E}}_i)]}{\log_2(k+1)})$ in Eq. (19), we model the link prediction procedure as 1) randomly select K nodes from the whole node space $\mathcal{V}$; 2) calculate $|\widetilde{\mathcal{E}}_i \cap \widehat{\mathcal{E}}_i|$, i.e., how many nodes among the selected nodes $\widetilde{\mathcal{E}}_i$ are in the ground-truth neighborhood list $\widehat{\mathcal{E}}_i$; 3) randomly select $|\widetilde{\mathcal{E}}_i \cap \widehat{\mathcal{E}}_i|$ slots to position nodes in $\widetilde{\mathcal{E}}_i \cap \widehat{\mathcal{E}}_i$ and calculate DCG. The above steps can be mathematically formulated as:

$$\sum_{i=0}^{K}\frac{C(N-\alpha d, K-i)C(\alpha d, i)}{C(N,K)}\sum_{j=1}^{C(K,i)} p(\mathbf{O}_j^{(K,i)})\sum_{k=1}^{K}\frac{\mathbb{1}[\mathbf{O}_{jk}^{(K,i)}=1]}{\log_2(k+1)}, \tag{20}$$

where $\mathbf{O}^{(K,i)} \in \{0,1\}^{C(K,i)\times K}$ represents all $C(K,i)$ possible positional indices of putting i nodes into K candidate slots. Specifically $\mathbf{O}_j^{(K,i)} \in \{0,1\}^K$ indicates the j^{th} positional configuration of i nodes where $\mathbf{O}_{jk}^{(K,i)} = 1$ if an node is positioned at k^{th} slot and $\mathbf{O}_{jk}^{(K,i)} = 0$ otherwise. Since our link predictor has no bias in positioning nodes in the K slots by Lemma 1, we have $p(\mathbf{O}_j^{(K,i)}) = \frac{1}{C(K,i)}$ and Eq. (20) can be transformed as:

$$\sum_{i=0}^{K} \frac{C(N-\alpha d, K-i)C(\alpha d, i)}{C(N,K)} \frac{1}{C(K,i)} \sum_{j=1}^{C(K,i)} \sum_{k=1}^{K} \frac{\mathbb{1}[\mathbf{O}_{jk}^{(K,i)} = 1]}{\log_2(k+1)}. \tag{21}$$

We know that only when the k^{th} slot is positioned a node can we have $\mathbf{O}_{jk}^{(K,i)} = 1$ and among the total $C(K,i)$ selections, every candidate slot $k \in \{1, 2, ..., K\}$ would be selected $C(K-1, i-1)$ times to position a node, which hence leads to:

$$\sum_{j=1}^{C(K,i)} \sum_{k=1}^{K} \frac{\mathbb{1}[\mathbf{O}_{jk}^{(K,i)} = 1]}{\log_2(k+1)} = \sum_{k=1}^{K} \frac{C(K-1, i-1)}{\log_2(k+1)}. \tag{22}$$

We then substitute Eq. (22) into Eq. (21) as:

$$\begin{aligned}
&\sum_{i=0}^{K} \frac{C(N-\alpha d, K-i)C(\alpha d, i)}{C(N,K)} \frac{1}{C(K,i)} \sum_{k=1}^{K} \frac{C(K-1,i-1)}{\log_2(k+1)} \\
=& \sum_{i=0}^{K} \frac{C(N-\alpha d, K-i)C(\alpha d, i)}{C(N,K)} \frac{C(K-1,i-1)}{C(K,i)} \sum_{k=1}^{K} \frac{1}{\log_2(k+1)}.
\end{aligned} \tag{23}$$

Further substituting Eq. (23) into Eq. (19), we finally get:

$$\begin{aligned}
E(\text{N}@K|d_i) &= \sum_{i=0}^{K} \frac{C(N-\alpha d, K-i)C(\alpha d, i)}{C(N,K)} \frac{C(K-1,i-1)}{C(K,i)} \\
&= \sum_{i=0}^{K} \frac{C(N-\alpha d, K-i)C(\alpha d, i)}{C(N,K)} \frac{\frac{(K-1)!}{(i-1)!(K-i)!}}{\frac{K!}{i!(K-i)!}} \\
&= \frac{1}{K} \underbrace{\sum_{i=0}^{K} i \frac{C(N-\alpha d, K-i)C(\alpha d, i)}{C(N,K)}}_{E(|\widetilde{\mathcal{E}}_i \cap \widehat{\mathcal{E}}_i|)} = \frac{1}{K}\frac{\alpha d}{N} * K = \frac{\alpha d}{N}
\end{aligned} \tag{24}$$

□

Based on Theorem 3, Precision, F1, and NDCG increase as node degree increases even when no observed links are used to train the link predictor, which informs the degree-related evaluation bias and causes the illusion that high-degree nodes are more advantageous than low-degree ones observed in some previous works (Li et al., 2021; Rahmani et al., 2022).

D.3 REWEIGHTING BY LP SCORE ENHANCE 1-LAYER TC

Theorem 4. *Taking the normalization term $g(|\mathcal{H}_i^1|, |\mathcal{H}_j^1|) = |\mathcal{H}_i^1|$ and also assume that higher link prediction score $\mathbf{S}_{ij}$ between v_i and its neighbor v_j corresponds to more number of connections between v_j and the neighborhood $\mathcal{N}_i^{\text{Train}}$, i.e., $\mathbf{S}_{ij} > \mathbf{S}_{ik} \rightarrow |\mathcal{N}_j^{1,\text{Train}} \cap \mathcal{N}_i^{1,\text{Train}}| > |\mathcal{N}_k^{1,\text{Train}} \cap \mathcal{N}_i^{1,\text{Train}}|, \forall v_j, v_k \in \mathcal{N}_i^{\text{Train},1}$, then we have:*

$$\widehat{C}_i^{1,\text{Train}} = \sum_{v_j \sim \mathcal{N}_i^{\text{Train}}} \frac{\mathbf{S}_{ij}|\mathcal{H}_i^1 \cap \mathcal{H}_j^1|}{|\mathcal{H}_i^1|} \geq \mathbb{E}_{v_j \sim \mathcal{N}_i^{\text{Train}}} \frac{|\mathcal{H}_i^1 \cap \mathcal{H}_j^1|}{|\mathcal{H}_i^1|} = C_i^{1,\text{Train}} \tag{25}$$

Proof. By definition, we have $\mathcal{H}_i^1 = \mathcal{N}_i^{1,\text{Train}}$, then the computation of 1-layer TC^{Train} is transformed as:

$$C_i^{1,\text{Train}} = \mathbb{E}_{v_j \sim \mathcal{N}_i^{\text{Train}}} I(\mathcal{S}_i^1, \mathcal{S}_j^1) = \mathbb{E}_{v_j \sim \mathcal{N}_i^{\text{Train}}} \frac{|\mathcal{N}_i^{\text{Train}} \cap \mathcal{N}_j^{\text{Train}}|}{|\mathcal{N}_i^{\text{Train}}|} = \frac{1}{|\mathcal{N}_i^{\text{Train}}|} \mathbb{E}_{v_j \sim \mathcal{N}_i^{\text{Train}}} (|\mathcal{N}_i^{\text{Train}} \cap \mathcal{N}_j^{\text{Train}}|). \tag{26}$$

On the other hand, we similarly transform weighted TC as:

$$\widehat{C}_i^{1,\text{Train}} = \frac{1}{|\mathcal{N}_i^{\text{Train}}|} \sum_{v_j \sim \mathcal{N}_i^{\text{Train}}} (\mathbf{S}_{ij} |\mathcal{N}_i^{\text{Train}} \cap \mathcal{N}_j^{\text{Train}}|). \tag{27}$$

By the relation that:

$$\mathbf{S}_{ij} > \mathbf{S}_{ik} \rightarrow |\mathcal{N}_j^{1,\text{Train}} \cap \mathcal{N}_i^{1,\text{Train}}| > |\mathcal{N}_k^{1,\text{Train}} \cap \mathcal{N}_i^{1,\text{Train}}|, \forall v_j, v_k \in \mathcal{N}_i^{\text{Train},1}, \tag{28}$$

Then we have:

$$\widehat{C}_i^{1,\text{Train}} \geq C_i^{1,\text{Train}} \tag{29}$$

□

Moreover, we include Figure 9 to illustrate the idea of enhancing TC via assigning higher weights to edges connecting neighbors that have higher connections to the whole neighborhoods. We can see in this case, weighted TC in Figure 9(a) is naturally higher than the one in Figure 9(b)

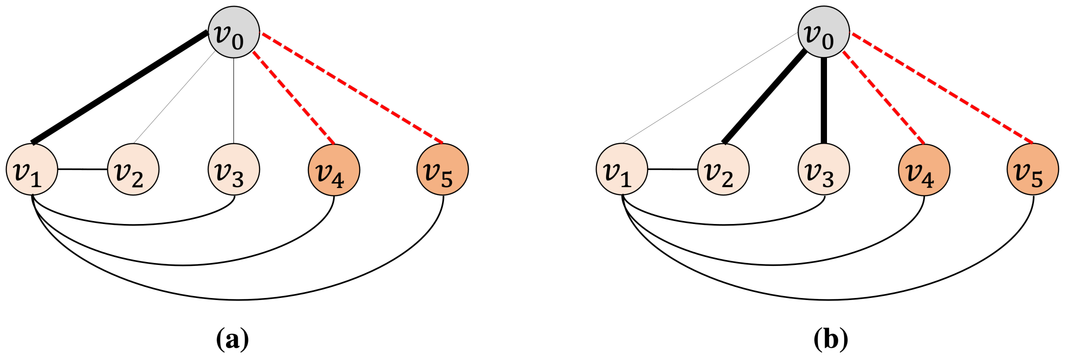

Figure 9: (a) Increasing the weight of neighbors that have more connections with the whole neighborhood while (b) increasing the weight of neighbors that have fewer connections with the whole neighborhood. (a) would increase the weighted TC while (b) would not

E EXAMPLE DEMONSTRATING THE ADVANTAGES OF TC OVER LCC

According to the definition of local clustering coefficient (LCC) and TC, we respectively calculate their values for node v_1 in Figure 10. v_2, v_3, v_4 do not have any connection among themselves, indicating node v_1 prefer interacting with nodes coming from significantly different domain/community. Subsequently, the incoming neighbors v_5, v_6 of v_1 are likely to also come from other communities and hence share no connections with v_2, v_3, v_4, which leads to the ill topological condition for predicting links of v_1. However, in this case, the clustering coefficient still maintains 0.5 because of the connections between v_1 and $v_2/v_3/v_4$, which cannot precisely capture the ill-topology of v_1 in this case. Conversely, our TC^{Train} equals 0, reflecting the ill topological condition of v_1.

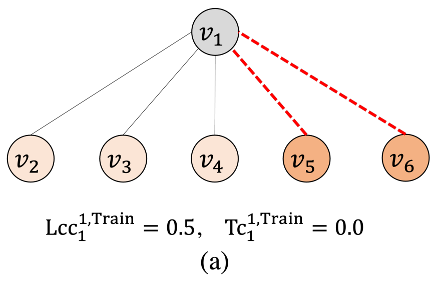
v_1
v_2
v_3
v_4
v_5
v_6
$\text{Lcc}_1^{1,\text{Train}} = 0.5$, $\text{Tc}_1^{1,\text{Train}} = 0.0$
(a)

Figure 10: Comparison of TC and LCC

F Datasets and Experimental Settings

This section introduces datasets and experimental settings used in this paper.

F.1 Dataset Introduction and Statistics

We use five widely employed datasets for evaluating the link prediction task, including four citation networks: Cora, Citeseer, Pubmed, and Citation2, and 1 human social network Collab. We further introduce two real-world animal social networks, Reptile and Vole, based on animal interactions.

- **Cora/Citeseer/Pubmed**: Following (Zhao et al., 2022; Chamberlain et al., 2022; Wang et al., 2023), we randomly split edges into 70%/10%/20% so that there is no topological distribution shift in these datasets. We use Hits@100 to evaluate the final performance.
- **Collab/Citation2**: We leverage the default edge splitting from OGBL (Hu et al., 2020). These two datasets mimic the real-life link prediction scenario where testing edges later joined in the network than validation edges and further than training edges. This would cause the topological distribution shift observed in the **Obs.3** of Section 3.3. For Collab, different from (Chamberlain et al., 2022; Wang et al., 2023), our setting does not allow validation edges to join the network for message-passing when evaluating link prediction performance. Therefore, the edges used for message-passing and supervision come from edges in the training set. In addition, we also consider a widely used setting in prior work where the validation edges would be allowed in message-passing when evaluating in the testing stage and we term this one on Collab as Collab* (Wang et al., 2023; Chamberlain et al., 2022).
- **Reptile/Vole**: we obtain the dataset from Network Repository (Rossi & Ahmed, 2015). To construct this network, a bipartite network was first constructed based on burrow use - an edge connecting a tortoise node to a burrow node indicated a burrow used by the individual. Social networks of desert tortoises were then constructed by the bipartite network into a single-mode projection of tortoise nodes. Node features are initialized by a trainable embedding layer, and we leverage the same edge splitting 70%/10%/20% for training/validation/testing.

Table 3: Statistic of datasets used for evaluating link prediction.

Network Domain	Dataset	# Nodes	# Edges	Split Type	Metric	Split Ratio
Citation Network	Cora	2,708	5,278	Random	Hits@100	70/10/20%
	Citeseer	3,327	4,676	Random	Hits@100	70/10/20%
	Pubmed	18,717	44,327	Random	Hits@100	70/10/20%
	Citation2	2,927,963	30,561,187	Time	MRR	Default
Social Network	Collab	235,868	1,285,465	Time	Hits@50	Default
Animal Network	Reptile	787	1232	Random	Hits@100	70/10/20%
	Vole	1480	3935	Random	Hits@100	70/10/20%

F.2 Hyperparameter Details

For all experiments, we select the best configuration on validation edges and report the model performance on testing edges. The search space for the hyperparameters of the GCN/SAGE/LightGCN baselines and their augmented variants GCN$_{rw}$/SAGE$_{rw}$ are: graph convolutional layer $\{1, 2, 3\}$, hidden dimension of graph encoder $\{64, 128, 256\}$, the learning rate of the encoder and predictor $\{0.001, 0.005, 0.01\}$, dropout $\{0.2, 0.5, 0.8\}$, training epoch $\{50, 100, 500, 1000\}$, batch size $\{256, 1152, 64 * 1024\}$ (Hu et al., 2020; Chamberlain et al., 2022; Wang et al., 2023), weights $\alpha \in \{0.5, 1, 2, 3, 4\}$, the update interval $\tau \in \{1, 2, 10, 20, 50\}$, warm up epochs $T^{\text{warm}} \in \{1, 2, 5, 10, 30, 50\}$. For baseline NCN[2], we directly run their code using their default best-performing configurations on Cora/Citeseer/Pubmed/Collab but for Citation2, due to memory limitation, we directly take the result from the original paper. We use cosine similarity metric as the similarity function ϕ in computing ATC.

[2]https://github.com/GraphPKU/NeuralCommonNeighbor

G Additional Results

To demonstrate that the observations made previously in Section 3 can also generalize to other datasets, here we present the comprehensive results on all datasets we study in this paper as follows.

G.1 Link prediction performance grouped by $\mathrm{TC}^{\mathrm{Test}}$

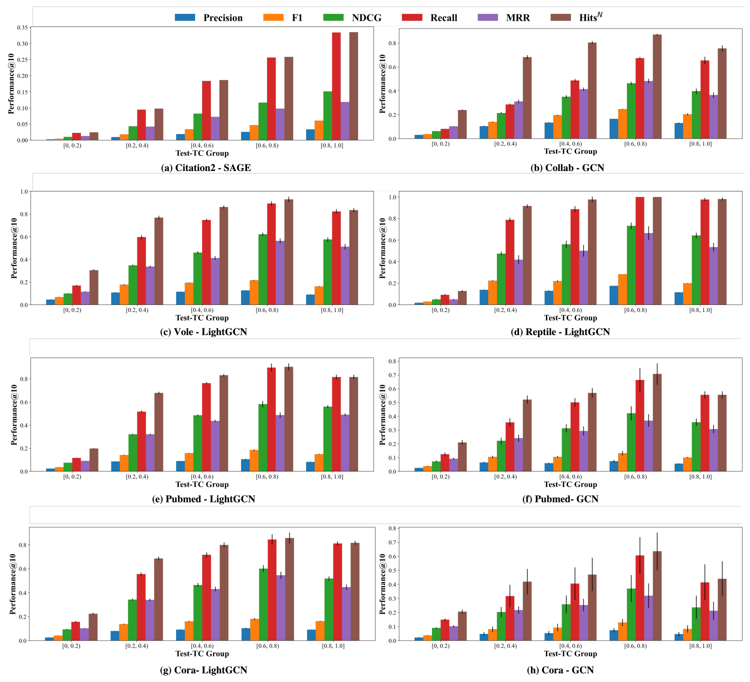

Figure 11: LP performance grouped by $\mathrm{TC}^{\mathrm{Test}}$ for all nodes

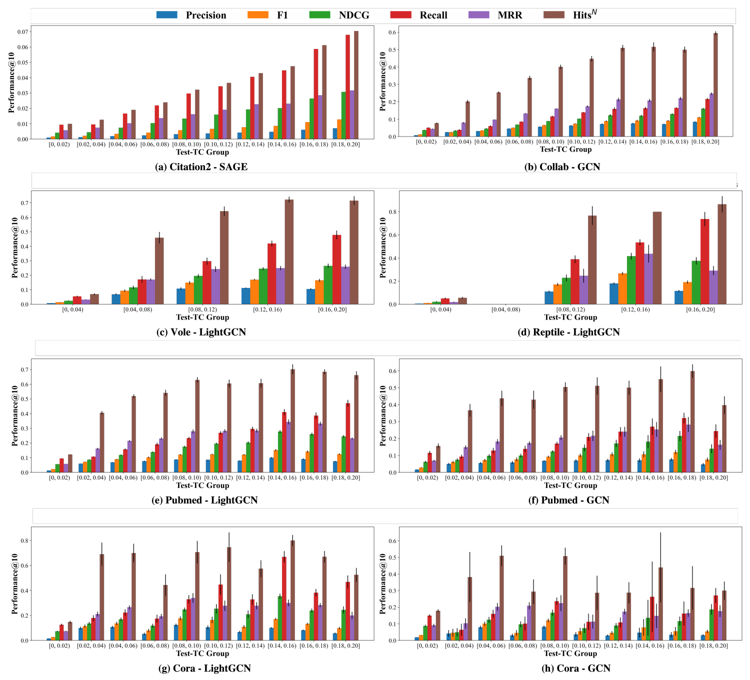

Figure 12: LP performance grouped by $\mathrm{TC}^{\mathrm{Test}}$ for low $\mathrm{TC}^{\mathrm{Test}}$ nodes

G.2 Link prediction performance grouped by $\mathrm{TC}^{\mathrm{Train}}$

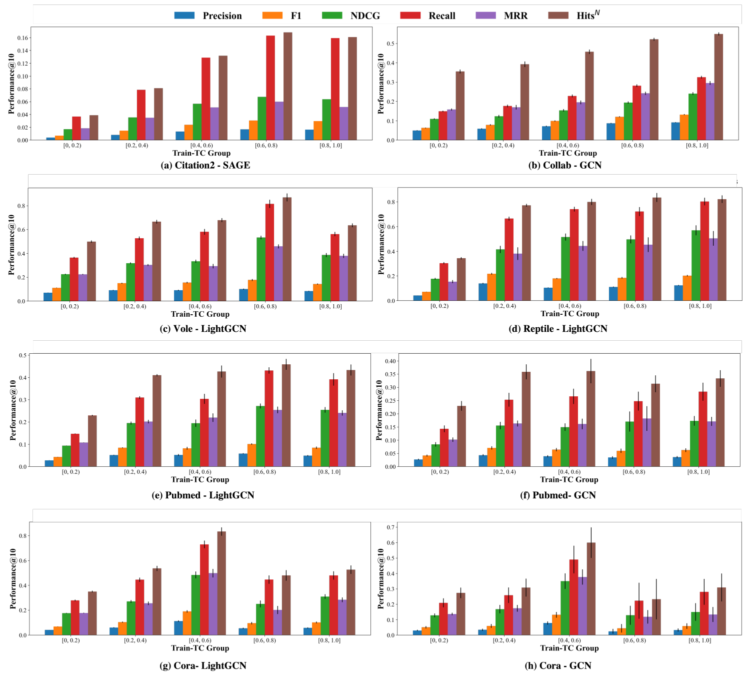

Figure 13: LP performance grouped by $\mathrm{TC}^{\mathrm{Train}}$ for all nodes

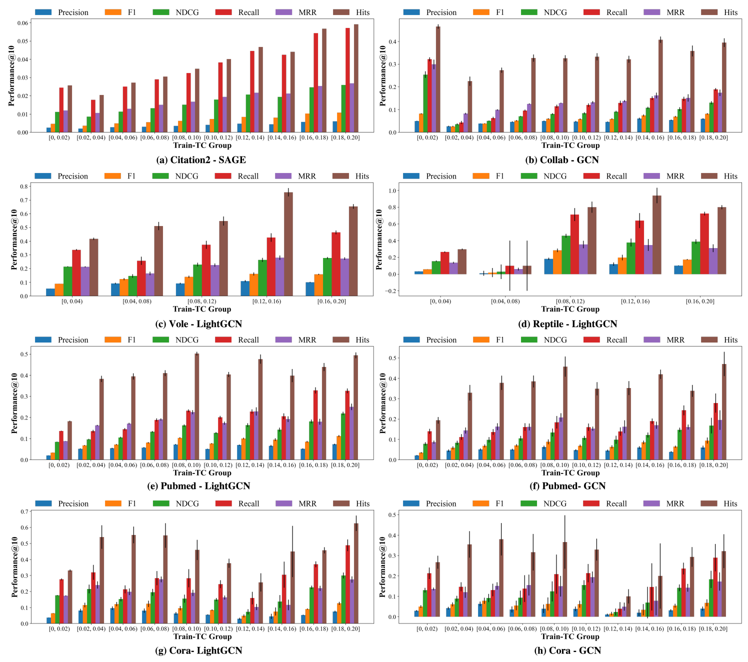

Figure 14: LP performance grouped by $\mathrm{TC}^{\mathrm{Train}}$ for low $\mathrm{TC}^{\mathrm{Train}}$ nodes

G.3 LINK PREDICTION PERFORMANCE GROUPED BY DEGREE$^{\text{Test}}$

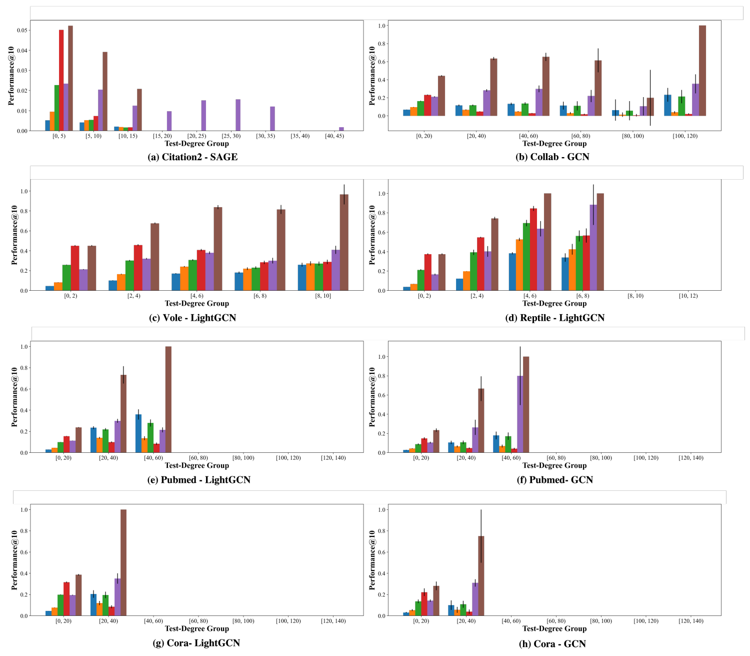

Figure 15: LP performance grouped by Degree$^{\text{Test}}$ for all nodes

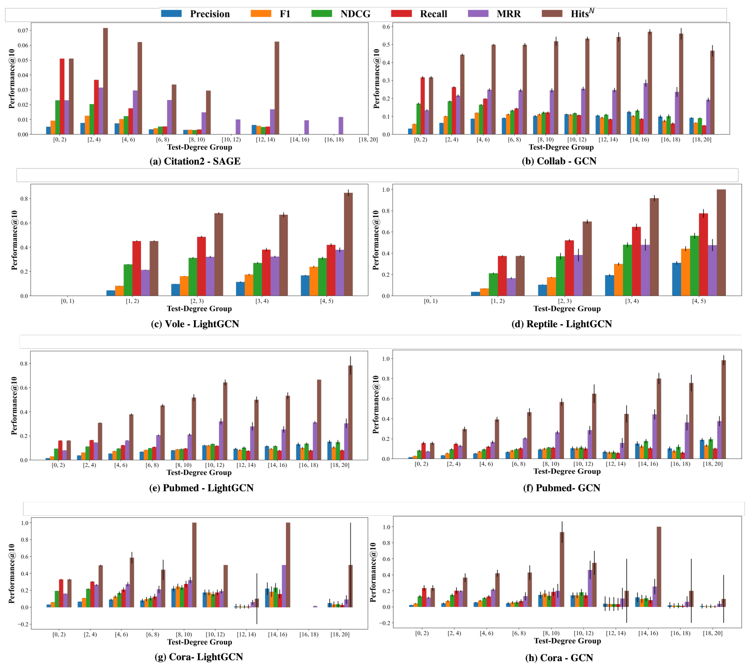

Figure 16: LP performance grouped by Degree$^{\text{Test}}$ for low Test-Degree nodes

G.4 Link prediction performance grouped by Degree$^{\text{Train}}$

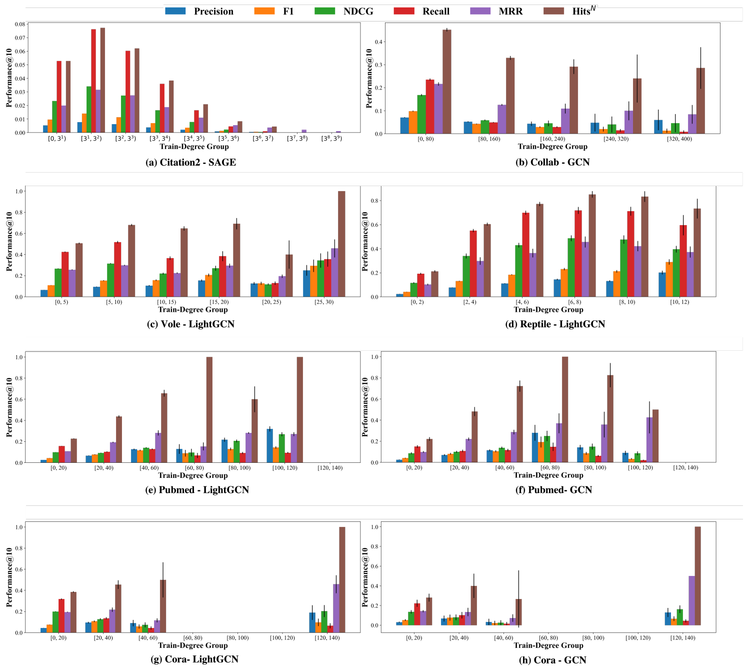

Figure 17: LP performance grouped by Degree$^{\text{Train}}$ for all nodes

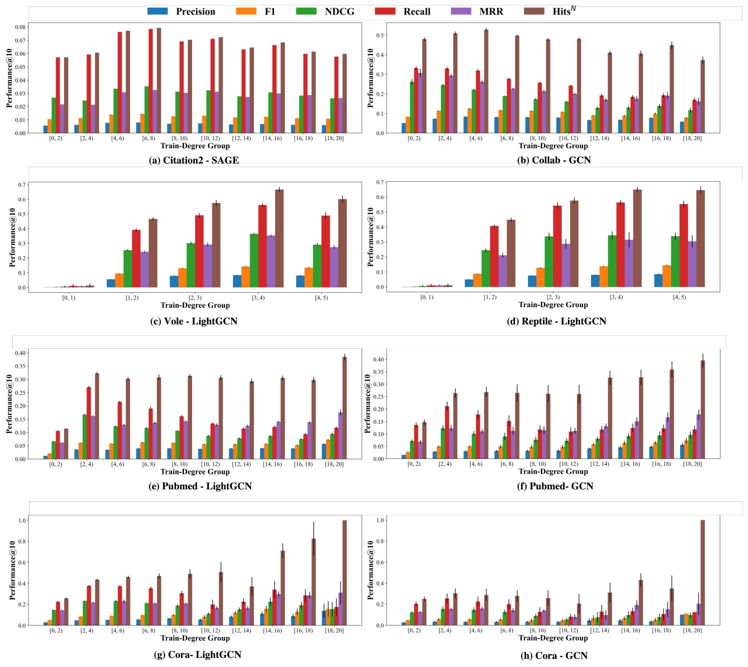

Figure 18: LP performance grouped by Degree$^{\text{Train}}$ for low Degree$^{\text{Train}}$ nodes

G.5 Relation between LP performance and TC at Graph-level

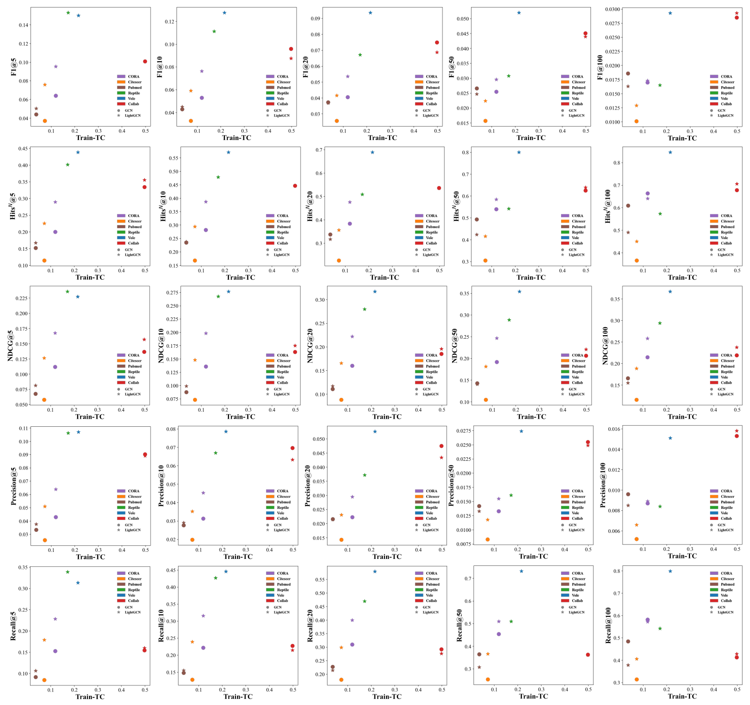

Figure 19: Relation between LP performance and TC at Graph-level

G.6 Relation between TC^{Train} and TC^{Test}

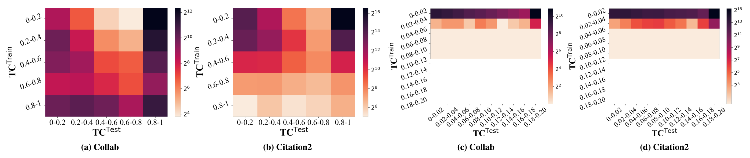

Figure 20: Relation between TC^{Train} and TC^{Test} on Collab/Citation2

G.7 Difference in TC vs Difference in Performance before/after applying reweighting

G.8 Correlation of the performance with TC and Degree

Here we present the comprehensive correlation of the performance with $\text{TC}^{\text{Train}}/\text{TC}^{\text{Val}}/\text{TC}^{\text{Test}}$ and $\text{Degree}^{\text{Train}}$. As the performance is evaluated under different K, we further define the absolute average/the typical average correlation across different K values to reflect the absolute correlation strength/the consistency of the correlation average:

$$\text{Absolute Avg.}_{X@K} = \frac{1}{4}\sum_{k\in\{5,10,20,50\}} |X@k|, \quad \text{Basic Avg.}_{X@K} = \frac{1}{4}\sum_{k\in\{5,10,20,50\}} X@k$$

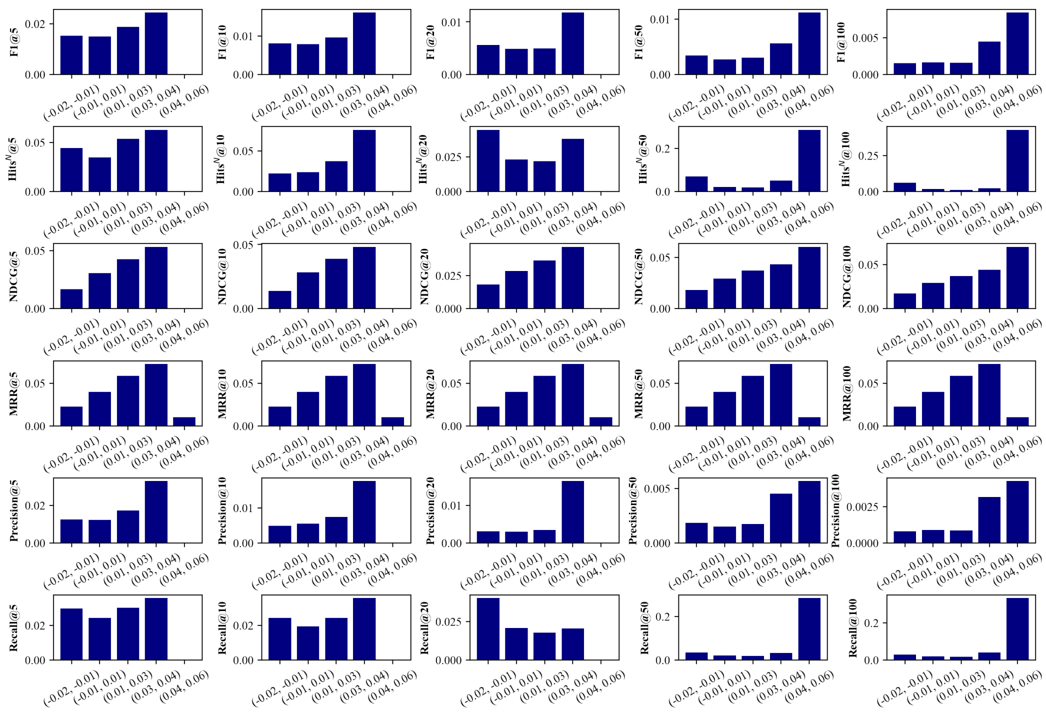

Figure 21: Relation between TC^{Train} and TC^{Test} on Collab by running GCN

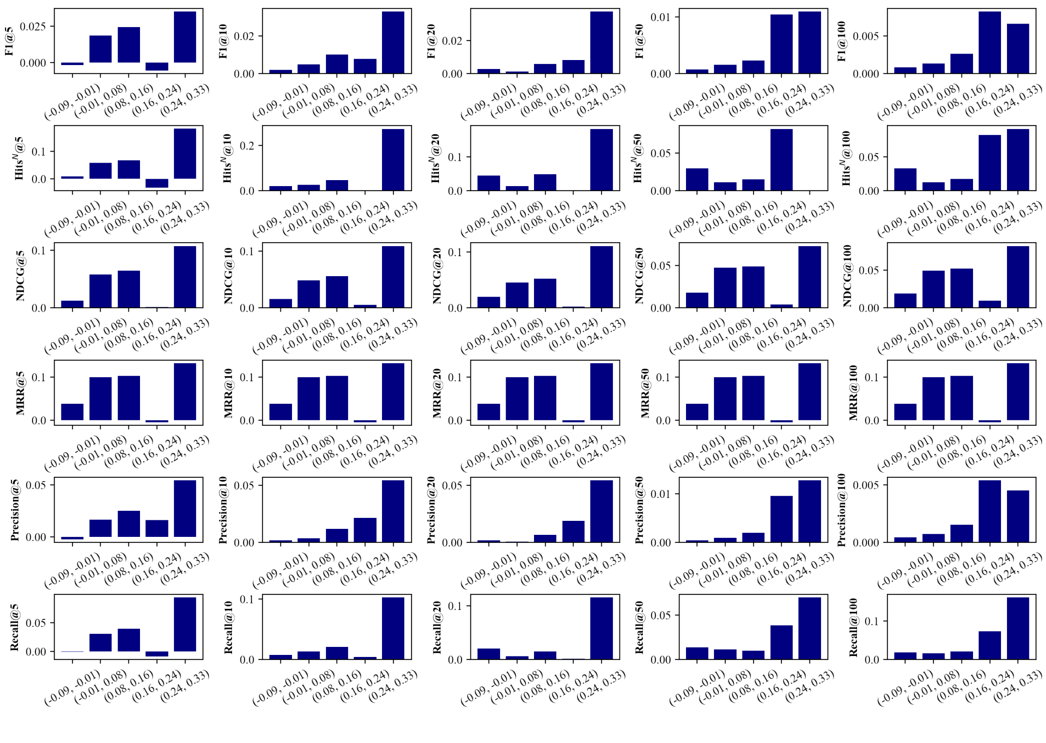

Figure 22: Relation between TC^{Train} and TC^{Test} on Collab by running SAGE

Table 4: The correlation between TC^{Train}/TC^{Val}/TC^{Test}/$\text{Degree}^{\text{Train}}$ and the GCN's LP performance on **Collab**. We note that the formal definitions of Absolute Avg. and Basic Avg. are provided in Section G.8 and they represent the average absolute and simple average correlation, respectively, across the range of @K for the given metric; these are also then calculated overall.

	Metric	@5	@10	@20	@50	Absolute Avg.	Basic Avg.
TC^{Train}	Precision	0.2252	0.1925	0.1353	0.0578	0.1527	0.1527
	F1	0.2601	0.2364	0.1733	0.0790	0.1872	0.1872
	NDCG	0.2279	0.2427	0.2375	0.2206	0.2322	0.2322
	Recall	0.2296	0.2358	0.2156	0.1754	0.2141	0.2141
	Hits^N	0.2057	0.1800	0.1328	0.0717	0.1476	0.1476
	MRR	0.2044				0.2044	0.2044
						0.1867	0.1867
TC^{Val}	Precision	0.2573	0.2832	0.2788	0.2387	0.2645	0.2645
	F1	0.2425	0.2901	0.2991	0.2641	0.2740	0.2740
	NDCG	0.2066	0.2330	0.2521	0.2624	0.2385	0.2385
	Recall	0.1742	0.2179	0.2428	0.2514	0.2216	0.2216
	Hits^N	0.2445	0.2674	0.2720	0.2620	0.2615	0.2615
	MRR	0.2350				0.2350	0.2350
						0.2520	0.2520
TC^{Test}	Precision	0.5184	0.5437	0.5107	0.4127	0.4964	0.4964
	F1	0.5858	0.6311	0.5964	0.4799	0.5733	0.5733
	NDCG	0.5443	0.6282	0.6706	0.6902	0.6333	0.6333
	Recall	0.5644	0.6753	0.7324	0.7533	0.6814	0.6814
	Hits^N	0.5272	0.5816	0.5924	0.5720	0.5683	0.5683
	MRR	0.5085				0.5085	0.5085
						0.5905	0.5905
$\text{Degree}^{\text{Train}}$	Precision	-0.1261	-0.0829	0.0006	0.1440	0.0884	-0.0161
	F1	-0.1997	-0.1663	-0.0813	0.0812	0.1321	-0.0915
	NDCG	-0.1822	-0.2017	-0.1985	-0.1750	0.1894	-0.1894
	Recall	-0.2183	-0.2288	-0.2118	-0.1681	0.2068	-0.2068
	Hits^N	-0.1395	-0.1164	-0.0658	0.0055	0.0818	-0.0791
	MRR	-0.1349				-0.1349	-0.1349
						0.1397	-0.1166
$\text{Degree}^{\text{Val}}$	Precision	0.0047	0.0472	0.1117	0.2141	0.0944	0.0944
	F1	-0.0823	-0.0469	0.0200	0.1416	0.0727	0.0081
	NDCG	-0.0608	-0.0803	-0.0838	-0.0736	0.0746	-0.0746
	Recall	-0.1203	-0.1296	-0.1269	-0.1100	0.1217	-0.1217
	Hits^N	-0.0063	0.0171	0.0481	0.0848	0.0391	0.0359
	MRR	-0.0108				-0.0108	-0.0108
						0.0805	-0.0116
$\text{Degree}^{\text{Test}}$	Precision	0.1075	0.1833	0.2924	0.4617	0.2612	0.2612
	F1	-0.0669	0.0043	0.1249	0.3375	0.1334	0.1000
	NDCG	-0.034	-0.0723	-0.0814	-0.0668	0.0636	-0.0636
	Recall	-0.1678	-0.1856	-0.187	-0.1724	0.1782	-0.1782
	Hits^N	0.0785	0.1103	0.1407	0.1718	0.1253	0.1253
	MRR	0.0727				0.0727	0.0727
						0.1524	0.0489
Subgraph Density	Precision	0.2199	0.1646	0.0875	-0.0073	0.1198	0.1162
	F1	0.2806	0.2259	0.1353	0.0161	0.1645	0.1645
	NDCG	0.2811	0.2891	0.2748	0.2491	0.2735	0.2735
	Recall	0.2911	0.2783	0.2399	0.1834	0.2482	0.2482
	Hits^N	0.2265	0.1842	0.1196	0.0423	0.1432	0.1432
	MRR	0.2331				0.2331	0.2331
						0.1898	0.1891

Table 5: The correlation between TC^{Train}/TC^{Val}/TC^{Test}/$\text{Degree}^{\text{Train}}$ and the GCN's LP performance on **Citation2**. We note that the formal definitions of Absolute Avg. and Basic Avg. are provided in Section G.8 and they represent the average absolute and simple average correlation, respectively, across the range of @K for the given metric; these are also then calculated overall.

	Metric	@5	@10	@20	@50	Absolute Avg.	Basic Avg.
TC^{Train}	Precision	0.0839	0.1312	0.1784	0.2157	0.1523	0.1523
	F1	0.0849	0.1323	0.1795	0.2165	0.1533	0.1533
	NDCG	0.0773	0.1164	0.1585	0.2012	0.1384	0.1384
	Recall	0.0860	0.1346	0.1845	0.2265	0.1579	0.1579
	Hits^N	0.0840	0.1314	0.1791	0.2182	0.1532	0.1532
	MRR		0.1229			0.1229	0.1229
						0.1510	0.1510
TC^{Val}	Precision	0.0575	0.0868	0.1200	0.1479	0.1031	0.1031
	F1	0.0581	0.0874	0.1206	0.1484	0.1036	0.1036
	NDCG	0.0545	0.0790	0.1078	0.1377	0.0948	0.0948
	Recall	0.0586	0.0884	0.1231	0.1540	0.1060	0.1060
	Hits^N	0.0574	0.0870	0.1206	0.1500	0.1038	0.1038
	MRR		0.0846			0.0846	0.0846
						0.1022	0.1022
TC^{Test}	Precision	0.1797	0.2541	0.3313	0.3996	0.2912	0.2912
	F1	0.1812	0.2558	0.3328	0.4008	0.2927	0.2927
	NDCG	0.1706	0.2365	0.3071	0.3825	0.2742	0.2742
	Recall	0.1829	0.2599	0.3401	0.4141	0.2993	0.2993
	Hits^N	0.1797	0.2550	0.3331	0.4048	0.2932	0.2932
	MRR		0.2512			0.2512	0.2512
						0.2901	0.2901
$\text{Degree}^{\text{Train}}$	Precision	-0.0288	-0.0406	-0.0536	-0.0689	0.0480	-0.0480
	F1	-0.0295	-0.0415	-0.0546	-0.0699	0.0489	-0.0489
	NDCG	-0.0285	-0.0394	-0.0522	-0.0692	0.0473	-0.0473
	Recall	-0.0305	-0.0436	-0.0589	-0.0791	0.0530	-0.0530
	Hits^N	-0.0289	-0.0408	-0.0540	-0.0708	0.0486	-0.0486
	MRR		-0.0421			-0.0421	-0.0421
						0.0492	0.0492
$\text{Degree}^{\text{Val}}$	Precision	0.0161	0.0229	0.0300	0.0393	0.0271	0.0271
	F1	0.0156	0.0220	0.0289	0.0381	0.0262	0.0262
	NDCG	0.0150	0.0199	0.0248	0.0305	0.0226	0.0226
	Recall	0.0150	0.0203	0.0252	0.0301	0.0227	0.0227
	Hits^N	0.0161	0.0232	0.0300	0.0384	0.0269	0.0269
	MRR		0.0234			0.0234	0.0234
						0.0251	0.0251
$\text{Degree}^{\text{Test}}$	Precision	0.0060	0.0113	0.0190	0.0364	0.0182	0.0182
	F1	-0.0009	0.0047	0.0128	0.0314	0.0125	0.0120
	NDCG	-0.0086	-0.0113	-0.0147	-0.0185	0.0133	-0.0133
	Recall	-0.0135	-0.0185	-0.0251	-0.0344	0.0229	-0.0229
	Hits^N	0.0051	0.0081	0.0120	0.0159	0.0103	0.0103
	MRR		0.0104			0.0104	0.0104
						0.0154	0.0009
Subgraph Density	Precision	0.0809	0.1217	0.1607	0.1916	0.1387	0.1387
	F1	0.0823	0.1231	0.1621	0.1926	0.1400	0.1400
	NDCG	0.0761	0.1111	0.1476	0.1853	0.1300	0.1300
	Recall	0.0842	0.1268	0.1691	0.2063	0.1466	0.1466
	Hits^N	0.0811	0.1219	0.1618	0.1956	0.1401	0.1401
	MRR		0.1144			0.1144	0.1144
						0.1391	0.1391

Table 6: The correlation between TC$^{\text{Train}}$/TC$^{\text{Val}}$/TC$^{\text{Test}}$/Degree$^{\text{Train}}$ and the GCN's LP performance on **Cora**. We note that the formal definitions of Absolute Avg. and Basic Avg. are provided in Section G.8 and they represent the average absolute and simple average correlation, respectively, across the range of @K for the given metric; these are also then calculated overall.

	Metric	@5	@10	@20	@50	Absolute Avg.	Basic Avg.
TC$^{\text{Train}}$	Precision	0.0985	0.1046	0.1238	0.1571	0.1210	0.1210
	F1	0.0989	0.1042	0.1239	0.1597	0.1217	0.1217
	NDCG	0.0933	0.0990	0.1088	0.1306	0.1079	0.1079
	Recall	0.1020	0.1042	0.1162	0.1568	0.1198	0.1198
	Hits^N	0.0961	0.1000	0.1226	0.1617	0.1201	0.1201
	MRR	0.0869				0.0869	0.0869
						0.1181	0.1181
TC$^{\text{Val}}$	Precision	0.0342	0.0456	0.0840	0.0903	0.0635	0.0635
	F1	0.0296	0.0406	0.0820	0.0907	0.0607	0.0607
	NDCG	0.0215	0.0259	0.0446	0.0526	0.0362	0.0362
	Recall	0.0257	0.0322	0.0724	0.0841	0.0536	0.0536
	Hits^N	0.0331	0.0413	0.0742	0.0932	0.0605	0.0605
	MRR	0.0291				0.0291	0.0291
						0.0549	0.0549
TC$^{\text{Test}}$	Precision	0.4694	0.4702	0.4667	0.3977	0.4510	0.4510
	F1	0.4952	0.4964	0.4948	0.4216	0.4770	0.4770
	NDCG	0.4970	0.5239	0.5551	0.5759	0.5380	0.5380
	Recall	0.4941	0.5109	0.5448	0.5347	0.5211	0.5211
	Hits^N	0.4749	0.4909	0.5130	0.4866	0.4914	0.4914
	MRR	0.4920				0.4920	0.4920
						0.4957	0.4957
Degree$^{\text{Train}}$	Precision	0.0751	0.0970	0.1701	0.3268	0.1673	0.1673
	F1	-0.0039	0.0237	0.0938	0.2549	0.0941	0.0921
	NDCG	-0.0156	-0.0276	-0.0283	-0.0191	0.0227	-0.0227
	Recall	-0.0432	-0.0547	-0.0568	-0.0529	0.0519	-0.0519
	Hits^N	0.0656	0.0650	0.0862	0.1135	0.0826	0.0826
	MRR	0.0307				0.0307	0.0307
						0.0837	0.0837
Degree$^{\text{Val}}$	Precision	0.0433	0.0623	0.1138	0.2248	0.1111	0.1111
	F1	-0.0230	0.0012	0.0508	0.1634	0.0596	0.0481
	NDCG	-0.0235	-0.0336	-0.0369	-0.0361	0.0325	-0.0325
	Recall	-0.0570	-0.0648	-0.0689	-0.0784	0.0673	-0.0673
	Hits^N	0.0253	0.0222	0.0308	0.0431	0.0304	0.0304
	MRR	0.0144				0.0144	0.0144
						0.0602	0.0179
Degree$^{\text{Test}}$	Precision	0.1669	0.2104	0.3046	0.4890	0.2927	0.2927
	F1	0.0537	0.1111	0.2127	0.4149	0.1981	0.1981
	NDCG	0.0004	-0.0104	-0.0082	0.0060	0.0063	-0.0031
	Recall	-0.0599	-0.0702	-0.0760	-0.0781	0.0711	-0.0711
	Hits^N	0.1406	0.1487	0.1624	0.1865	0.1596	0.1596
	MRR	0.1116				0.1116	0.1116
						0.1455	0.1153
Subgraph Density	Precision	0.0794	0.0900	0.0796	0.0381	0.0718	0.0718
	F1	0.1088	0.1189	0.1066	0.0580	0.0981	0.0981
	NDCG	0.1157	0.1378	0.1543	0.1674	0.1438	0.1438
	Recall	0.1330	0.1690	0.2015	0.2272	0.1827	0.1827
	Hits^N	0.0851	0.1109	0.1257	0.1385	0.1151	0.1151
	MRR	0.0976				0.0976	0.0976
						0.1223	0.1223

Table 7: The correlation between TC^{Train}/TC^{Val}/TC^{Test}/$\text{Degree}^{\text{Train}}$ and the GCN's LP performance on **Citeseer**. We note that the formal definitions of Absolute Avg. and Basic Avg. are provided in Section G.8 and they represent the average absolute and simple average correlation, respectively, across the range of @K for the given metric; these are also then calculated overall.

	Metric	@5	@10	@20	@50	Absolute Avg.	Basic Avg.
TC^{Train}	Precision	0.3330	0.3735	0.3898	0.3830	0.3698	0.3698
	F1	0.3324	0.3803	0.4056	0.4049	0.3808	0.3808
	NDCG	0.2831	0.3226	0.3570	0.3879	0.3377	0.3377
	Recall	0.3001	0.3481	0.3920	0.4295	0.3674	0.3674
	Hits^N	0.3386	0.3901	0.4287	0.4603	0.4044	0.4044
	MRR	0.3194				0.3194	0.3194
						0.3720	0.3720
TC^{Val}	Precision	0.2796	0.2962	0.3224	0.3229	0.3053	0.3053
	F1	0.2756	0.2947	0.3291	0.3365	0.3090	0.3090
	NDCG	0.2508	0.2662	0.2929	0.3118	0.2804	0.2804
	Recall	0.2491	0.2585	0.2928	0.3086	0.2773	0.2773
	Hits^N	0.2801	0.3049	0.338	0.3496	0.3182	0.3182
	MRR	0.2763				0.2763	0.2763
						0.2980	0.2980
TC^{Test}	Precision	0.6786	0.698	0.6745	0.6220	0.6683	0.6683
	F1	0.7157	0.7385	0.7207	0.6678	0.7107	0.7107
	NDCG	0.7037	0.7540	0.7946	0.8300	0.7706	0.7706
	Recall	0.7299	0.7797	0.8258	0.8588	0.7986	0.7986
	Hits^N	0.7127	0.7595	0.7979	0.8216	0.7729	0.7729
	MRR	0.7070				0.7070	0.7070
						0.7442	0.7442
$\text{Degree}^{\text{Train}}$	Precision	0.2472	0.3523	0.4591	0.5861	0.4112	0.4112
	F1	0.1867	0.2727	0.3872	0.5408	0.3469	0.3469
	NDCG	0.1303	0.1645	0.2022	0.2475	0.1861	0.1861
	Recall	0.1144	0.1532	0.2047	0.2591	0.1829	0.1829
	Hits^N	0.2538	0.3181	0.3581	0.3886	0.3297	0.3297
	MRR	0.2227				0.2227	0.2227
						0.2913	0.2913
$\text{Degree}^{\text{Val}}$	Precision	0.1431	0.1866	0.2255	0.277	0.2081	0.2081
	F1	0.1147	0.1582	0.2053	0.2693	0.1869	0.1869
	NDCG	0.0845	0.1014	0.1194	0.1429	0.1121	0.1121
	Recall	0.0693	0.0880	0.1113	0.1411	0.1024	0.1024
	Hits^N	0.1438	0.1683	0.1857	0.2148	0.1782	0.1782
	MRR	0.1366				0.1366	0.1366
						0.1575	0.1575
$\text{Degree}^{\text{Test}}$	Precision	0.3052	0.4412	0.5704	0.7223	0.5098	0.5098
	F1	0.1919	0.3133	0.4639	0.6597	0.4072	0.4072
	NDCG	0.0949	0.1220	0.1548	0.1975	0.1423	0.1423
	Recall	0.0323	0.0562	0.0909	0.1314	0.0777	0.0777
	Hits^N	0.2745	0.3258	0.3378	0.3369	0.3188	0.3188
	MRR	0.2444				0.2444	0.2444
						0.2911	0.2911
Subgraph Density	Precision	0.1559	0.1412	0.1168	0.0858	0.1249	0.1249
	F1	0.1867	0.1699	0.1420	0.1035	0.1505	0.1505
	NDCG	0.2006	0.2097	0.2176	0.2235	0.2129	0.2129
	Recall	0.2218	0.2289	0.2411	0.2491	0.2352	0.2352
	Hits^N	0.1768	0.1799	0.1982	0.2097	0.1912	0.1912
	MRR	0.1759				0.1759	0.1759
						0.1829	0.1829

Table 8: The correlation between TC^{Train}/TC^{Val}/TC^{Test}/$Degree^{Train}$ and the GCN's LP performance on **Pubmed**. We note that the formal definitions of Absolute Avg. and Basic Avg. are provided in Section G.8 and they represent the average absolute and simple average correlation, respectively, across the range of @K for the given metric; these are also then calculated overall.

	Metric	@5	@10	@20	@50	Absolute Avg.	Basic Avg.
TC^{Train}	Precision	0.1981	0.2358	0.2681	0.2924	0.2486	0.2486
	F1	0.1690	0.2216	0.2652	0.2961	0.2380	0.2380
	NDCG	0.1195	0.1379	0.1600	0.1831	0.1501	0.1501
	Recall	0.0917	0.1142	0.1336	0.1397	0.1198	0.1198
	$Hits^N$	0.1932	0.2267	0.2485	0.2513	0.2299	0.2299
	MRR	0.1920				0.1920	0.1920
						0.1973	0.1973
TC^{Val}	Precision	0.1769	0.2180	0.2653	0.3134	0.2434	0.2434
	F1	0.1253	0.1815	0.2462	0.3092	0.2156	0.2156
	NDCG	0.0780	0.0846	0.1046	0.1303	0.0994	0.0994
	Recall	0.0417	0.0503	0.0672	0.0804	0.0599	0.0599
	$Hits^N$	0.1627	0.1882	0.2068	0.2077	0.1914	0.1914
	MRR	0.1607				0.1607	0.1607
						0.1619	0.1619
TC^{Test}	Precision	0.3769	0.3989	0.4078	0.3909	0.3936	0.3936
	F1	0.4011	0.4258	0.4329	0.4088	0.4172	0.4172
	NDCG	0.3902	0.4231	0.4547	0.4870	0.4388	0.4388
	Recall	0.3809	0.4080	0.4286	0.4335	0.4128	0.4128
	$Hits^N$	0.3923	0.4247	0.4463	0.4436	0.4267	0.4267
	MRR	0.4097				0.4097	0.4097
						0.4178	0.4178
$Degree^{Train}$	Precision	0.2433	0.3108	0.3761	0.4849	0.3538	0.3538
	F1	0.1019	0.1970	0.2987	0.4456	0.2608	0.2608
	NDCG	0.0477	0.0366	0.0441	0.0715	0.0500	0.0500
	Recall	-0.0402	-0.0386	-0.0385	-0.0357	0.0383	-0.0383
	$Hits^N$	0.2080	0.2404	0.2504	0.2612	0.2400	0.2400
	MRR	0.2051				0.2051	0.2051
						0.1886	0.1733
$Degree^{Val}$	Precision	0.1823	0.2290	0.2849	0.3681	0.2661	0.2661
	F1	0.0676	0.1368	0.2220	0.3359	0.1906	0.1906
	NDCG	0.0293	0.0164	0.0221	0.0407	0.0271	0.0271
	Recall	-0.0429	-0.0466	-0.0459	-0.0476	0.0458	-0.0458
	$Hits^N$	0.1536	0.1749	0.1831	0.1872	0.1747	0.1747
	MRR	0.1573				0.1573	0.1573
						0.1408	0.1225
$Degree^{Test}$	Precision	0.3073	0.3898	0.4719	0.6133	0.4456	0.4456
	F1	0.1251	0.2423	0.3716	0.5624	0.3254	0.3254
	NDCG	0.0588	0.0406	0.0480	0.0821	0.0574	0.0574
	Recall	-0.0537	-0.0565	-0.0605	-0.0575	0.0571	-0.0571
	$Hits^N$	0.2615	0.2966	0.3030	0.3099	0.2928	0.2928
	MRR	0.2556				0.2556	0.2556
						0.2356	0.2128
Subgraph Density	Precision	0.1002	0.0746	0.0414	-0.0146	0.0577	0.0504
	F1	0.1732	0.1319	0.0792	0.0030	0.0968	0.0968
	NDCG	0.2146	0.2307	0.2357	0.2344	0.2289	0.2289
	Recall	0.2475	0.2547	0.2540	0.2428	0.2498	0.2498
	$Hits^N$	0.1343	0.1330	0.1338	0.1288	0.1325	0.1325
	MRR	0.1430				0.1430	0.1430
						0.1531	0.1517

Table 9: The correlation between TC^{Train}/TC^{Val}/TC^{Test}/$\text{Degree}^{\text{Train}}$ and the GCN's LP performance on **Vole**. We note that the formal definitions of Absolute Avg. and Basic Avg. are provided in Section G.8 and they represent the average absolute and simple average correlation, respectively, across the range of @K for the given metric; these are also then calculated overall.

	Metric	@5	@10	@20	@50	Absolute Avg.	Basic Avg.
TC^{Train}	Precision	0.2725	0.2710	0.2648	0.2287	0.2593	0.2593
	F1	0.2985	0.2981	0.2869	0.2401	0.2809	0.2809
	NDCG	0.2714	0.3012	0.3300	0.3497	0.3131	0.3131
	Recall	0.2946	0.3267	0.3677	0.3917	0.3452	0.3452
	Hits^N	0.3113	0.3307	0.3694	0.3988	0.3526	0.3526
	MRR	0.2721				0.2721	0.2721
						0.3102	0.3102
TC^{Val}	Precision	0.1375	0.1717	0.1847	0.1721	0.1665	0.1665
	F1	0.1233	0.1690	0.1871	0.1739	0.1633	0.1633
	NDCG	0.0931	0.1201	0.1403	0.1479	0.1254	0.1254
	Recall	0.0825	0.1251	0.1570	0.1548	0.1299	0.1299
	Hits^N	0.1347	0.1558	0.1815	0.1814	0.1634	0.1634
	MRR	0.1219				0.1219	0.1219
						0.1497	0.1497
TC^{Test}	Precision	0.5547	0.4822	0.3937	0.2527	0.4208	0.4208
	F1	0.6498	0.5597	0.4449	0.2742	0.4822	0.4822
	NDCG	0.7395	0.7712	0.7954	0.8030	0.7773	0.7773
	Recall	0.7325	0.7384	0.7367	0.6812	0.7222	0.7222
	Hits^N	0.6470	0.6529	0.6452	0.6016	0.6367	0.6367
	MRR	0.6950				0.6950	0.6950
						0.6078	0.6078
$\text{Degree}^{\text{Train}}$	Precision	0.2103	0.2728	0.3620	0.4508	0.3240	0.3240
	F1	0.1387	0.2253	0.3391	0.4508	0.2885	0.2885
	NDCG	0.0180	0.0352	0.0760	0.1222	0.0629	0.0629
	Recall	0.0238	0.0479	0.1111	0.1993	0.0955	0.0955
	Hits^N	0.1688	0.1977	0.2551	0.2989	0.2301	0.2301
	MRR	0.0512				0.0512	0.0512
						0.2002	0.2002
$\text{Degree}^{\text{Val}}$	Precision	0.0312	0.0747	0.1182	0.1758	0.1000	0.1000
	F1	-0.0135	0.0414	0.0989	0.1685	0.0806	0.0738
	NDCG	-0.0527	-0.0455	-0.0336	-0.0153	0.0368	-0.0368
	Recall	-0.0670	-0.0487	-0.0309	0.0059	0.0381	-0.0352
	Hits^N	0.0077	0.0180	0.0368	0.0599	0.0306	0.0306
	MRR	-0.0215				-0.0215	-0.0215
						0.0572	0.0265
$\text{Degree}^{\text{Test}}$	Precision	0.3731	0.5111	0.6562	0.8126	0.5883	0.5883
	F1	0.2040	0.3944	0.5926	0.7916	0.4957	0.4957
	NDCG	0.0004	0.0257	0.0722	0.1330	0.0578	0.0578
	Recall	-0.0942	-0.0697	-0.0301	0.0419	0.0590	-0.0380
	Hits^N	0.2320	0.2604	0.2731	0.2529	0.2546	0.2546
	MRR	0.1642				0.1642	0.1642
						0.2911	0.2717
Subgraph Density	Precision	0.0744	0.0369	-0.0119	-0.0815	0.0512	0.0045
	F1	0.1372	0.0860	0.0187	-0.0689	0.0777	0.0433
	NDCG	0.2205	0.2341	0.2398	0.2398	0.2336	0.2336
	Recall	0.2178	0.2366	0.2495	0.2545	0.2396	0.2396
	Hits^N	0.1206	0.1493	0.1688	0.2138	0.1631	0.1631
	MRR	0.2026				0.2026	0.2026
						0.1530	0.1368

Table 10: The correlation between TC$^{\text{Train}}$/TC$^{\text{Val}}$/TC$^{\text{Test}}$/Degree$^{\text{Train}}$ and the GCN's LP performance on **Reptile**. We note that the formal definitions of Absolute Avg. and Basic Avg. are provided in Section G.8 and they represent the average absolute and simple average correlation, respectively, across the range of @K for the given metric; these are also then calculated overall.

	Metric	@5	@10	@20	@50	Absolute Avg.	Basic Avg.
TC$^{\text{Train}}$	Precision	0.5189	0.5084	0.4977	0.5009	0.5065	0.5065
	F1	0.5420	0.5307	0.5146	0.5090	0.5241	0.5241
	NDCG	0.5298	0.5502	0.5636	0.5741	0.5544	0.5544
	Recall	0.5097	0.5176	0.5343	0.5475	0.5273	0.5273
	Hits^{N}	0.5208	0.5278	0.5407	0.5502	0.5349	0.5349
	MRR	0.5300				0.5300	0.5300
						0.5294	0.5294
TC$^{\text{Val}}$	Precision	0.3994	0.4316	0.4550	0.4647	0.4377	0.4377
	F1	0.3753	0.4250	0.4573	0.4670	0.4312	0.4312
	NDCG	0.3183	0.3535	0.3790	0.3909	0.3604	0.3604
	Recall	0.2670	0.3085	0.3525	0.3744	0.3256	0.3256
	Hits^{N}	0.3213	0.3483	0.3675	0.3840	0.3553	0.3553
	MRR	0.3666				0.3666	0.3666
						0.3820	0.3820
TC$^{\text{Test}}$	Precision	0.7083	0.7000	0.6739	0.6506	0.6832	0.6832
	F1	0.7898	0.7629	0.7138	0.6678	0.7336	0.7336
	NDCG	0.8475	0.8897	0.9029	0.9072	0.8868	0.8868
	Recall	0.8573	0.8858	0.8931	0.8759	0.8780	0.8780
	Hits^{N}	0.8276	0.8566	0.8604	0.8495	0.8485	0.8485
	MRR	0.8163				0.8163	0.8163
						0.8060	0.8060
Degree$^{\text{Train}}$	Precision	0.4998	0.5294	0.5664	0.5947	0.5476	0.5476
	F1	0.5082	0.5411	0.5788	0.6017	0.5575	0.5575
	NDCG	0.4247	0.4572	0.4914	0.5120	0.4713	0.4713
	Recall	0.4338	0.4598	0.5201	0.5615	0.4938	0.4938
	Hits^{N}	0.4998	0.5073	0.5391	0.5664	0.5282	0.5282
	MRR	0.4369				0.4369	0.4369
						0.5197	0.5197
Degree$^{\text{Val}}$	Precision	0.3185	0.3577	0.3797	0.3924	0.3621	0.3621
	F1	0.3022	0.3546	0.3840	0.3956	0.3591	0.3591
	NDCG	0.2285	0.2617	0.2858	0.2985	0.2686	0.2686
	Recall	0.1997	0.2384	0.2830	0.3093	0.2576	0.2576
	Hits^{N}	0.2729	0.2938	0.3165	0.3339	0.3043	0.3043
	MRR	0.2677				0.2677	0.2677
						0.3103	0.3103
Degree$^{\text{Test}}$	Precision	0.6833	0.7492	0.7935	0.8118	0.7595	0.7595
	F1	0.5477	0.6726	0.7556	0.7968	0.6932	0.6932
	NDCG	0.3062	0.3404	0.3676	0.3790	0.3483	0.3483
	Recall	0.1840	0.2103	0.2429	0.2532	0.2226	0.2226
	Hits^{N}	0.3940	0.3555	0.3381	0.3283	0.3540	0.3540
	MRR	0.4468				0.4468	0.4468
						0.4755	0.4755
Subgraph Density	Precision	0.2482	0.2491	0.2211	0.2022	0.2302	0.2302
	F1	0.2943	0.2849	0.2420	0.2108	0.2580	0.2580
	NDCG	0.3560	0.3819	0.3792	0.3765	0.3734	0.3734
	Recall	0.3588	0.3928	0.3777	0.3607	0.3725	0.3725
	Hits^{N}	0.3440	0.3891	0.3837	0.3745	0.3728	0.3728
	MRR	0.3510				0.3510	0.3510
						0.3214	0.3214

H Edge Reweighting Algorithm

Here we present our edge reweigting algorithm to enhance the link prediction performance by modifying the graph adjacency matrix in message-passing. We normalize the adjacency matrix to get $\widetilde{\mathbf{A}}$ and $\widehat{\mathbf{A}}$ as defined in the algorithm below.

Algorithm 1: Edge Reweighting to Boost LP performance

```
Input: The input training graph $(\mathbf{A}, \mathbf{X}, \mathcal{E}^{\text{Train}}, \mathbf{D})$, graph encoder $f_{\mathbf{\Theta}_f}$, link predictor $g_{\mathbf{\Theta}_g}$, update interval
       $\Delta$, training epochs $T$, warm up epochs $T^{\text{warm}}$ and weights $\gamma$ for combining the original adjacency
       matrix and the updated adjacency matrix. The validation adjacency/degree matrix $\mathbf{A}^{\text{Val}}$/$\mathbf{D}^{\text{Val}}$ that
       only includes edges in the validation set.
1  Compute the normalized adjacency matrices $\widehat{\mathbf{A}} = \mathbf{D}^{-0.5}\mathbf{A}\mathbf{D}^{-0.5}$, $\widetilde{\mathbf{A}} = \mathbf{D}^{-1}\mathbf{A}$, $\widetilde{\mathbf{A}}^{\text{Val}} = \mathbf{D}^{\text{Val}^{-1}}\mathbf{A}^{\text{Val}}$
2  $\widetilde{\mathbf{A}}^0 = \widehat{\mathbf{A}}$
3  for $\tau = 1, \dots, T$ do
4      if $\tau\%\Delta \neq 0$ or $\tau \leq T^{\text{warm}}$ then
5          $\widetilde{\mathbf{A}}^\tau = \widetilde{\mathbf{A}}^{\tau-1}$
       /* Message-passing and LP to update model parameters */
6      for mini-batch of edges $\mathcal{E}^b \subseteq \mathcal{E}^{\text{Train}}$ do
7          Sample negative edges $\mathcal{E}^{b,-}$, s.t., $|\mathcal{E}^{b,-}| = |\mathcal{E}^b|$
8          Compute node embeddings $\mathbf{H}^\tau = f_{\mathbf{\Theta}_f^{\tau-1}}(\widetilde{\mathbf{A}}^\tau, \mathbf{X})$
9          Compute link prediction scores $\mathbf{E}_{ij}^\tau = g_{\mathbf{\Theta}_g^{\tau-1}}(\mathbf{H}_i^\tau, \mathbf{H}_j^\tau), \forall (i,j) \in \mathcal{E}^b \cup \mathcal{E}^{\text{Train}}$
10         $\mathcal{L}^{b,\tau} = -\frac{1}{|\mathcal{E}^b|}(\sum_{e_{ij} \in \mathcal{E}^b} \log \mathbf{E}_{ij}^\tau + \sum_{e_{mn} \in \mathcal{E}^{b,-}} \log(1 - \mathbf{E}_{mn}^\tau))$
11         Update $\mathbf{\Theta}_g^\tau \leftarrow \mathbf{\Theta}_g^{\tau-1} - \nabla_{\mathbf{\Theta}_g^{\tau-1}}\mathcal{L}^{b,\tau}$,  $\mathbf{\Theta}_f^\tau \leftarrow \mathbf{\Theta}_f^{\tau-1} - \nabla_{\mathbf{\Theta}_f^{\tau-1}}\mathcal{L}^{b,\tau-1}$
       /* Update adjacency matrix to enhance weighted TC */
12     if $\tau\%\Delta == 0$ and $\tau > T^{\text{warm}}$ then
13         Compute node embeddings $\mathbf{H}^\tau = f_{\mathbf{\Theta}_f^{\tau-1}}(\widetilde{\mathbf{A}}^{\tau-1}, \mathbf{X})$;
14         if Using training neighbors to reweigh then
15             Average pooling the neighborhood embeddings $\mathbf{N}^\tau = \widetilde{\mathbf{A}}\mathbf{H}^\tau$
16         if Using validation neighbors to reweigh then
17             Average pooling the neighborhood embeddings $\mathbf{N}^\tau = \widetilde{\mathbf{A}}^{\text{Val}}\mathbf{H}^\tau$
18         Compute the link prediction scores $\mathbf{S}_{ij}^\tau = \frac{\exp(g_{\mathbf{\Theta}_g^\tau}(\mathbf{N}_i^\tau, \mathbf{H}_j^\tau))}{\sum_{j=1}^n \exp(g_{\mathbf{\Theta}_g^\tau}(\mathbf{N}_i^\tau, \mathbf{H}_j^\tau))}$
19         Update the adjacency matrix $\widetilde{\mathbf{A}}^\tau \leftarrow \widehat{\mathbf{A}} + \gamma\mathbf{S}^\tau$
20 Return: $\widetilde{\mathbf{A}}^\tau, f_{\mathbf{\Theta}_f^\tau}, g_{\mathbf{\Theta}_g^\tau}$
```

I Reweigh edges for baselines without message-passing

As discussed in Section 4, we enhance node TC$^{\text{Train}}$ by reweighing the edges in message-passing. However, for some state-of-the-art baselines Chamberlain et al. (2022) that directly employ the neural transformation rather than message-passing to obtain node embeddings, we reweigh edges in computing the binary cross entropy loss in the training stage as follows:

$$\mathcal{L} = -\frac{1}{|\mathcal{E}^b|} \sum_{e_{ij \in \mathcal{E}^b}} (w_{ij} \sum_{e_{ij} \in \mathcal{E}^b} \log \mathbf{E}_{ij}^\tau + w_{mn} \sum_{e_{mn} \in \mathcal{E}^{b,-}} \log(1 - \mathbf{E}_{mn}^\tau)), \tag{30}$$

where $w_{ij} = \sigma(\phi(\mathbf{N}_i, \mathbf{N}_j))$ quantifies the edge weight between v_i and v_j with σ being the Sigmoid function and ϕ being the cosine similarity. $\mathbf{N}_i$ is the node embedding of v_i obtained in Eq. (2).

Table 11: Comparing the efficiency (s) between X and our proposed X_{rw}.

Baseline	Cora	Citeseer	Pubmed	Collab	Reptile	Vole
GCN	19,5	15.5	158.4	2906	18.3	53.8
GCN_{rw}	21.1	17.2	158.5	2915	17.0	53.0
SAGE	22.3	17.0	189.8	2970	20.9	61.2
SAGE_{rw}	23.8	20.5	192.4	2982	21.7	61.9
BUDDY	3.41	4.51	15.51	906.18	2.50	4.99
BUDDY_{rw}	3.98	4.92	14.56	907.52	2.62	5.06

J Comparing the Efficiency between baseline and their augmented version by TC

Here we compare the running time (s) of each baseline and their corresponding augmented version by uniformly testing them on the same machine in Table 11. We can see that equipping our proposed reweighting strategy could enhance the performance but only lead to marginal computational overhead. This is because firstly, we only change the weight of existing edges and hence the number of edge weights to be calculated is linear to the network size. Secondly, we leverage the pre-computed node embeddings to compute the edge weights. Thirdly, we only periodically update the edge weights.

K Reweighting training neighbors based on their connections to training neighbors or validation neighbors

As discussed in **Obs. 3**, due to the topological distribution shift, the newly joined neighbors of one node become less and less connective to the previous neighbors of that node. Therefore, the training neighbors of one node share fewer connections with the testing neighbors of that node than the validation neighbors. This motivates us to further improve our reweighting strategy based on validation neighbors rather than training neighbors. **The intuition is that when performing message-passing to aggregate training neighbors' information for each node, we want to incorporate those training neighbors with more connections to that node's validation neighbors instead of those training neighbors with more connections to that node's training neighbors.** Technically, we include additional steps 14-17 to consider two scenarios in Algorithm H: **(1)** reweighting based on the connections of training neighbors to training neighbors and **(2)** reweighting based on the connections of training neighbors to validation neighbors. We experiment on Collab to compare the performance of these two scenarios in Table 12. We can see the performance of reweighting based on validation neighbors is higher than reweighting based on training neighbors. This demonstrates that the validation neighbors are more connected to the testing neighbors, justifying the existence of the topological distribution shift.

Table 12: Comparing the link prediction performance on Collab between reweighting based on training neighbors and reweighting based on validation neighbors

Performance	**GCN**			**SAGE**		
	No	**Train**	**Val**	**No**	**Train**	**Val**
Hits@5	18.94±1.20	<u>19.48±0.75</u>	**22.36±0.32**	11.25±1.24	<u>20.52±2.35</u>	**24.34±0.07**
Hits@10	31.24±3.44	<u>32.69±1.00</u>	**35.15±2.42**	26.41±1.88	<u>31.23±3.52</u>	**37.15±2.44**
Hits@50	50.12±0.22	<u>52.77±1.00</u>	**53.24±0.22**	49.68±0.25	<u>51.87±0.10</u>	**52.69±0.26**
Hits@100	54.44±0.49	<u>56.89±0.17</u>	**57.28±0.10**	54.69±0.18	<u>56.59±0.19</u>	**57.27±0.25**

L EXPLAINING WHY THE CURVE OF LINK PREDICTION PERFORMANCE HAS SEVERAL FAST DOWN IN FIGURE 7(A)

Here we delve deep into the reason why we encounter several fast-down performances in Figure 7(a). We ascribe it to the weight clip [3]. We hypothesize that the loss landscape has several local minimums and hence by weight clipping with higher upper bound constraints, our learning step would be also larger so that the model could jump out of its original local optimum and keep finding some other better local optimum, which corresponds to the fast downtrend (first jump away from one local minimum and then find another better local minimum). We further empirically verify our hypothesis by visualizing the performance curve for each training process with different clipping weights in Figure 23. We can clearly see that as the clipping threshold becomes lower (upper bound decreases), we observe less fast downtrend decreases.

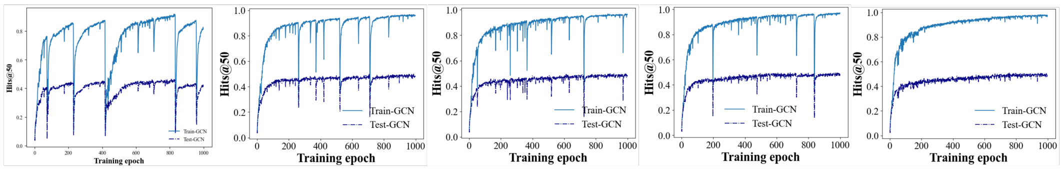

(a) No Clip (b) Clip 1.5 (c) Clip 1.0 (d) Clip 0.5 (d) Clip 0.2

Figure 23: From left to right, we constrain GCN-based link predictor with fewer upper bounds by clipping using a lower threshold. We can see the number of performance fast downtrend decreases. We hypothesize that the loss landscape has several local minimums and hence by weight clipping with lower upper bounds, our learning step would be also smaller so that the model could not jump out of its origin local optimum and hence we end up with fewer fast downtrends.

[3] Following the publically available implementation on GCN/SAGE on Collab link prediction, we employ the weight clip every time after parameter update